Monitoring vegetation dynamics with open earth observation tools: the case of fire-modulated savanna to forest transitions in Central Africa

Le Bienfaiteur Sagang Takougoum, Pierre Ploton, Gaëlle Viennois, Jean-Baptiste Féret, Bonaventure Sonké, Pierre Couteron, Nicolas Barbier

Title:

Monitoring vegetation dynamics with open earth observation tools: the case of fire-modulated savanna to forest transitions in Central Africa

Authors:
Sagang Takougoum Le Bienfaiteur[1,2,3,4], Ploton Pierre[2], Viennois Gaëlle[2], Féret Jean-Baptiste[5], Sonké Bonaventure[1,3], Couteron Pierre[2], Nicolas Barbier[2].
[1]Plant Systematics and Ecology Laboratory (LaBosystE), Department of Biology, Higher Teachers' Training College, University of Yaoundé I, Yaoundé. P.O. Box 047, Cameroon.
[2]AMAP, Univ Montpellier, IRD, CNRS, INRAE, CIRAD, 34394 Montpellier, France.
[3]International Joint Laboratory DYCOFAC, IRD-UYI-IRGM, Yaoundé. P.O Box 1857, Cameroon.
[4]Institute of Agricultural Research for Development, Njombe, Cameroon.
[5]TETIS, Irstea, CIRAD, CNRS, Univ Montpellier, Montpellier, France.

Correspondence:
Sagang T. Le Bienfaiteur
sagang.bienfaiteur@yahoo.fr

Abstract

Woody encroachment and forest progression are widespread in forest-savanna transitional areas in Central Africa. Quantifying these dynamics and understanding their drivers at relevant spatial scales has long been a challenge. Recent progress in open access imagery sources with improved spatial, spectral and temporal resolution combined with cloud computing resources, and the advent of relatively cheap solutions to deploy laser sensors in the field, have transformed this domain of study. We present a study case in the Mpem & Djim National Park (MDNP), a 1,000 km² protected area in the Centre region of Cameroon. Using open source algorithms in Google Earth Engine (GEE), we characterized vegetation dynamics and the fire regime based on Landsat multispectral imagery archive (1975-2020). Current species assemblages were estimated from Sentinel 2 imagery and the open source biodivMapR package, using spectral dissimilarity. Vegetation structure (aboveground biomass; AGB) was characterized using Unmanned Aerial vehicle (UAV) LiDAR scanning data sampled over the study area. Savanna vegetation, which was initially dominant in the MDNP, lost about 50% of its initial cover in less than 50 years in favor of forest at an average rate of ca. 0.63%.year^{-1} (6 km².year^{-1}). Species assemblage computed from spectral dissimilarity in forest vegetation followed a successional gradient consistent with forest age. AGB accumulation rate was 3.2 Mg.ha^{-1}.year^{-1} after 42 years of forest encroachment. In savannas, two modes could be identified along the gradient of spectral species assemblage, corresponding to distinct AGB levels, where woody savannas with low fire frequency store 40% more AGB than open grassy

savannas with high fire frequency. A fire occurrence every five year was found to be the fire regime threshold below which woody savannas start to dominate over grassy ones. A fire frequency below that threshold opens the way to young forest transitions. These results have implications for carbon sequestration and biodiversity conservation policies. Maintaining savanna ecosystems in the region would require active management actions to limit woody encroachment and forest progression, in contradiction with global reforestation goals.

Keywords: Forest-savanna transition, Google Earth Engine, fire, UAV-LiDAR, aboveground biomass, species assemblage.

1. Introduction

Understanding long term ecosystem dynamics, their drivers and effects on ecosystem state at a given point in time is a major challenge in ecology (Bastin et al., 2019; Estes et al., 2018; Valentini et al., 2014). Transitional areas between tropical forests and savannas form a widespread ecotone separating two of the most productive terrestrial ecosystems (Beer et al., 2010). Within a rather large domain of environmental conditions, both systems constitute alternative stable states (Hirota et al., 2011), each one generating the feedback loops ensuring its own maintenance. However, under all sufficiently wet climates where annual rainfall exceeds ≈ 650 mm, water availability is sufficient for woody canopy closure but disturbance mechanisms inherent to savannas, notably fire suppress trees and allow for their coexistence with grasses (Aleman et al., 2020; Sankaran et al., 2005; Staver et al., 2011b, 2011a). This balance has likely been shifted by ongoing climate change, as long term woody encroachment and forest progression into savannas have been described for forest-savanna ecotones (FSE) in Central Africa (Mitchard and Flintrop, 2013; Stevens et al., 2017, 2016; Youta-Happi et al., 2003).

These dynamics induce profound changes in ecosystem function and composition (Oliveras and Malhi, 2016; Zeng et al., 2013). Although tropical forests benefit from a good public image because of their high tree diversity (Sosef et al., 2017; Sullivan et al., 2017), aboveground carbon stocks (Mitchard et al., 2011; Santoro et al., 2021; Sullivan et al., 2017) and attributed aesthetic value (Niklas and Spatz, 2010; Panshin and De Zeeuw, 1980), they do not replace the specific fauna and flora of savannas, not to mention savanna's consequent belowground carbon stock (Blaum et al., 2007; Buisson et al., 2019; Sirami et al., 2009; Veldman et al., 2015). Moreover it will likely take centuries to attain a successional stage giving the newly formed forests a level of biomass and a floristic composition typical of old growth forests (Rüger et al., 2020). Conversely, recovering a typical grassland/savanna structure and composition, exempt

of invasive exotic species, may prove very difficult (Cava et al., 2020, 2018; Machida et al., 2021). Woody encroachment and forest progression at the expanse of savannas is thus neither desirable from the viewpoint of climate change mitigation policies, like the Bonn Challenge and the Reducing Emissions from Deforestation and Degradation (REDD+) initiative nor from that of the biotope conservation or restoration agenda (Abreu et al., 2017; Dinerstein et al., 2020; Thomas et al., 2013). The main questions a manager needs to answer are therefore: 1/ what are the tipping points for bush encroachment and forest transition in the current climatic conditions, considering the main mitigating tool at his disposal: the fire regime; 2/ what are the consequences of past ecosystem dynamics on the current distribution of carbon and biodiversity.

If field data provide an irreplaceable level of detail, notably for the characterization of vegetation structure and composition, they rarely provide the spatial and temporal hindsight necessary to understand ecosystem dynamics at a relevant scale. Currently available remote sensing approaches bring complementary and unique answers to the above questions. Thanks to its potential capacity for systematic observations at various scales, remote sensing (RS) offers practical and economical means to study vegetation cover changes over several decades, especially for large areas (Xie et al., 2019). Long term satellite imagery archives are now available globally, at a relatively high spatial and temporal resolution (Landsat, and now Sentinel 2) as well as open-access storage and computing facilities, such as the Google Earth Engine (GEE) computing platform (Gorelick et al., 2017). With these game-changing tools it is easy to monitor the transition from one biome to another, especially those with distinct spectral signatures as forest and savanna (DeVries et al., 2015; Dutrieux et al., 2015), at a meaningful spatiotemporal scale (Banskota et al., 2014). Mapping fire scars, which leave conspicuous and relatively long lasting marks in the landscape is also relatively easy (Daldegan et al., 2019, 2014; Liu et al., 2018) even using imagery with imperfect radiometric and atmospheric corrections.

Characterizing more subtle changes in species composition or vegetation structure (biomass), requires other data sources and algorithms. The Sentinel 2 constellation, carrying optical sensors of improved temporal, spectral and spatial resolutions have shown interesting prospects for detecting compositional gradients in the vegetation, notably in terms of the abundance of broad functional/optical plant types (Grabska et al., 2019; Ma et al., 2019). The unsupervised method for spectral species diversity analysis proposed by Féret and Asner (2014) for instance, provides preliminary assessment of such compositional gradients, loosely referred to as spectral

dissimilarity gradient (analogous to β-diversity), which could prove useful to detect sharp compositional changes occurring within transitioning pixels at the forest-savanna boundary, notably. However the capability of passive optical sensors to discriminate aboveground biomass (AGB) gradients is limited, especially in dense forests where AGB density frequently exceeds 200 Mg ha^{-1} (Jha et al., 2020; Sagang et al., 2020). Airborne LiDAR has become the reference method for the characterization of vegetation structure (Duncanson et al., 2021), but cost can be prohibitive. The arrival on the market of low-cost LiDAR scanners, which can be carried on Unmanned Aerial Vehicles (UAV), is now democratizing this crucial tool for vegetation structure assessment in tropical countries.

The objective of this study is twofold: the first aim is to advance our understanding of the dynamics and drivers of forest-savanna transitions, and their consequences in terms of above-ground carbon storage and tree species diversity. The second aim is to provide land managers (conservationists, as well as infrastructure investors in need for science-based compensation strategies) with reliable open tools allowing them to quantify the impact of different management strategies on ecosystem dynamics. To this end we combined the historical perspective on forest-savanna transition and fire regime provided by the Landsat archive to current day maps of spectral β-diversity and UAV-LiDAR derived AGB maps to obtain a coherent framework that could be generalized to similar transition areas for supporting and complementing traditional field campaigns. Our underlying hypotheses were the following: 1/ changes in fire regimes induce woody encroachment and forest transition below a specific fire frequency threshold; 2/ forest transition age results in changes in species composition and AGB detectable using integrative remote sensing data.

2. Methods

2.1. Study area

The study was conducted within the Mpem & Djim National Park (MDNP) located in a forest savanna mosaic of the Guineo-Congolian transitional area in the Centre region of Cameroon (Fig. 1). The MDNP was established in 2004 and covers an area of ca. 1,000 km². The area is under the influence of an equatorial climate of Guinean type (Djoufack, 2011), which is hot and humid with an average annual temperature of 25°C. Mean annual rainfall is 1,500 mm (Djoufack, 2011), with a rainfall distribution characterized by a five months dry season (November-March), during which the monthly rainfall is less than 70 mm per month. Soils are deep, mostly ferralitic red and yellow with a complete hydrolysis of minerals from granite-gneissic basement caused by warm rains (Santoir and Bopda, 1995). Savannas in the MDNP

are interspersed by semi-deciduous forests or gallery forests along watercourses (Letouzey, 1985; Youta-Happi et al., 2003; Youta-Happi and Bonvallot, 1996).

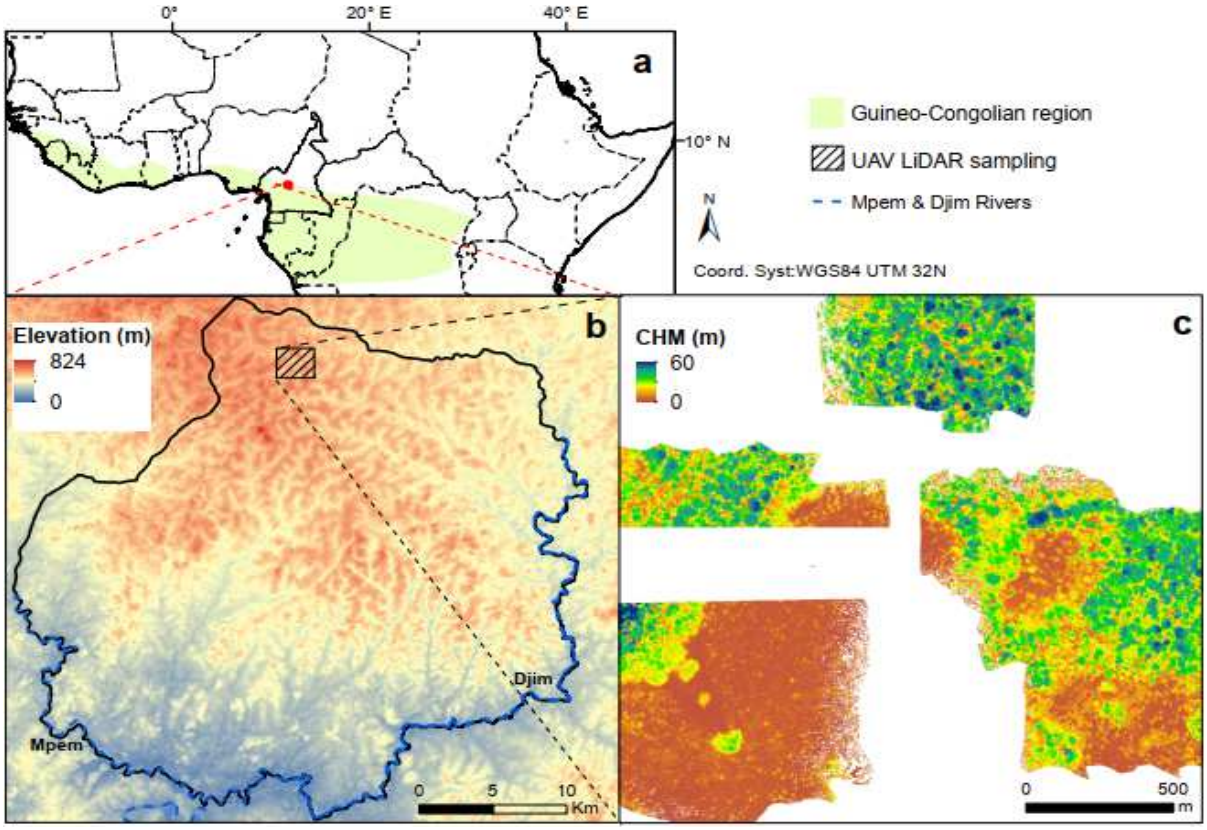

Fig. 1: Study area. (**a**) Location (red point) within the Guineo-Congolian transitional area (light green) and (**b**) boundaries of the Mpem & Djim National Park (full black polygon) following Mpem and Djim rivers (overlapping blue dashed lines). (**c**) UAV LiDAR-derived Canopy Height Model (CHM) at a 1m spatial resolution collected in the area (low areas in orange and higher ones in dark blue).

Tree species dominating young colonizing forests in direct contact with savanna are *Alchornea cordifolia* (Schumach. & Thonn.) Müll.Arg., *Albizia zygia* (DC.) J.F.Macbr., *Albizia adianthifolia* (Schumach.) W.Wight and *Albizia ferruginea* (Guill. & Perr.) Benth., *Macaranga spinosa* Müll. Arg., while emergent trees species such as *Mansonia altissima* (A.Chev.) A.Chev., *Terminalia superba* Engl. & Diels. and *Triplochiton scleroxylon* K. Schum., dominate in older forest successions. A distinct set of mostly pyrophilous tree species characterizes the savanna, mainly: *Annona senegalensis* Pers., *Bridelia ferruginea* Benth., *Crossopterix febrifuga* (Afzel. ex G.Don) Benth., *Hymenocardia lyrata* Tul., *Lannea kerstingii* (Enql.) K. Krause., *Terminalia glaucescens* Planch. ex Benth., *Piliostigma thonningii* (Schumach.) Milne-Redh., *Psorospermum febrifugum* Spach.. The grass cover is dominated by species of the Poaceae family: *Hyparrhenia diplandra* (Hack.) Stapf., *Hyparrhenia rufa* (Nees.) Stapf., *Pennisetum purpureum* Schumach. and *Andropogon spp.* (Youta-Happi, 1998).

2.2. Workflow of the analysis

The general workflow of the analysis is shown in Fig. 2 and can be grouped into three chunks.

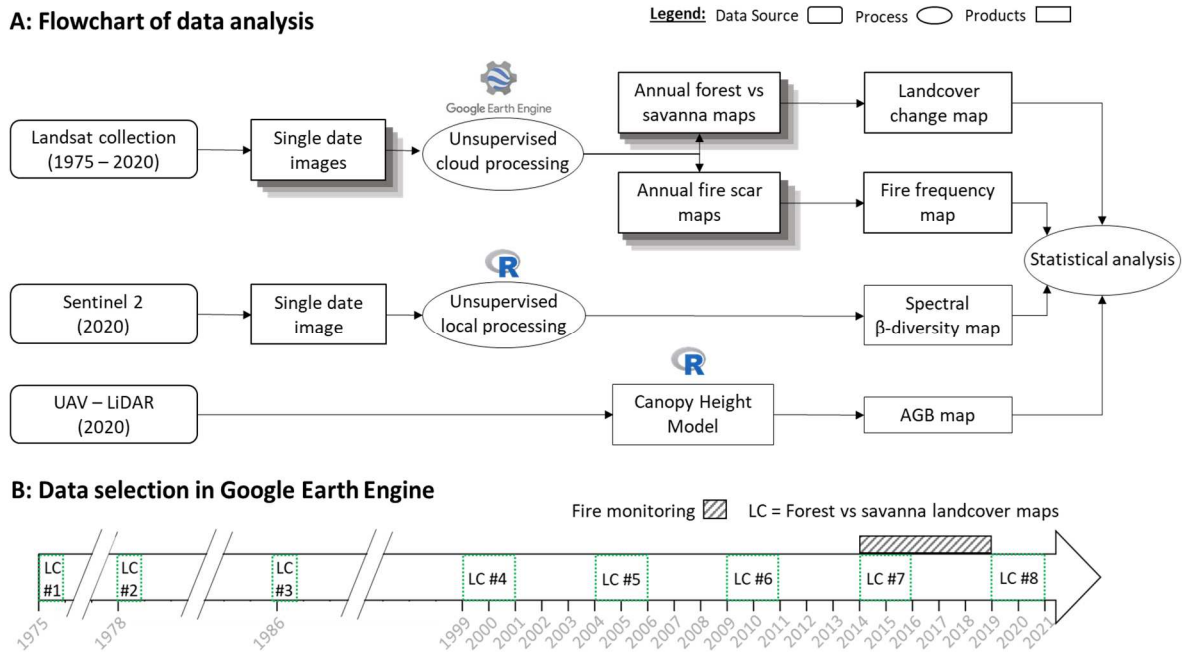

Fig. 2: Methodological workflow used in this study (A) and temporal domains covered by spaceborne data for vegetation and fire monitoring (B).

The first chunk includes the mapping of historical forest-savanna dynamics over the study area. The second chunk includes the mapping of the spatial distribution of fire frequency, and the third chunk includes the mapping of present-day vegetation diversity and biomass levels (Section A of Fig. 2). We used the GEE platform to access and preprocess (i.e., clouds and cloud shadows filtering) all spaceborne optical data. To map the historical forest-savanna dynamics, we leveraged Landsat archives from 1975 to 2020 and used automated (unsupervised) processing routines in GEE to generate a landcover change map (Section B of Fig. 2; see section 2.3 for a full description of the method). To assess the effect of fire on forest-savanna dynamics, a fire frequency map based on Landsat archives from 2014 to 2019 was generated using a semi-automated classification (see section 2.4). Fire regimes derived from Landsat were also compared to those derived from the MODIS burned area product. The assessment of present-day vegetation diversity gradients in the MDNP vegetation was based on a Sentinel 2 image from 2020, following the unsupervised spectral diversity analysis described in Féret and Boissieu (2020, see section 2.5.1). Last, we used UAV-borne LiDAR scanning (UAV-LS) data acquired in 2019 to map present-day vegetation biomass stocks (see section 2.5.2).

2.3. Mapping landcover changes

2.3.1. Temporal aggregation

There are three common strategies to process archive imagery collections for landcover monitoring (Banskota et al., 2014; Gómez et al., 2016; Nguyen et al., 2020). The simplest one consists in using individual, high quality cloud free scenes. In tropical, frequently cloudy conditions, this approach can prove difficult. The second alternative, where sufficient archive is available, is to generate temporal aggregates around pivot dates, allowing the use of information contained in partially cloudy images, at the expense of a reduced precision on the timing of detected changes (Hansen et al., 2013). Finally for dense temporal time series, pixel-level temporal analysis can be performed (Hermosilla et al., 2015) to optimize the use of the available data and the temporal precision of event detections. In this study, we were interested in the temporal hindsight, and therefore had to deal with very sparse series prior to the launch of Landsat 7 and 8 (and due to the long absence of ground stations in Africa). The third approach was thus excluded. Moreover, a major difficulty lies in inter-image heterogeneity induced by directional and atmospheric effects, although correction models are now routinely applied to recover bottom-of-atmosphere reflectance (such as the LEDAPS algorithm for Landsat 5 to 8 TM, ETM and OLI data collections produced by USGS, 2020). To work around the spectral stability issue, different approaches can be taken for image classification, mirroring the temporal aggregation choices summarized above: (i) train a classifier for each image, either manually, or automatically, if the landcover classes are sufficiently distinct, (ii) use the time redundancy (i.e. the similarity between successive temporal version of the pixels) to stabilize the signal at the scene level by time-aggregating a sufficient number of images or classifications (Souverijns et al., 2020), (iii) use the time redundancy to stabilize the signal at pixel level, to classify stable landcover classes between major breakpoint events (Verbesselt et al., 2010).

2.3.2. Automated-unsupervised landcover mapping

We developed an automated-unsupervised landcover mapping pipeline in GEE. Performing landcover classification directly on GEE is appealing in that it alleviates data transfer between the GEE platform and the operator. Besides, the use of unsupervised classification - which does not require human inputs for the processing of each single image - together with the massive computational capabilities of GEE, offers prospects for large-scale landcover mapping, provided that the unsupervised algorithm can accurately predict the landcover classes of interest. In the very convenient case of forest-savanna mosaics, the spectral contrast between

the two classes is so important, with highly bi-modal radiometric distribution in most spectral bands (see Appendix A). Therefore landcover classification can easily be performed automatically at the individual image level. This is true as long as clouds, cloud shadows and strong haze can be masked, as well as very distinct landcover classes such as water bodies and urban areas. Preliminary testing suggested that a simple k-means algorithm with two clusters successfully separated the two classes. On each image passing through the pipeline, we thus randomly selected 10,000 pixels to train a k-means algorithm and predicted the class of each remaining pixel using the NDVI. K-means classification was applied on single date images acquired before 1999 to generate the first three landcover maps (LC # 1 to 3 in section B of Fig. 2). For images acquired after 1999, K-means classifications of individual images were aggregated within the same 2-years intervals as in section 2.3.2 (LC # 4 to 8), by keeping the modal class of each pixel across images within time intervals. This resulted into eight binary forest (value of 1) and savanna (value of 0) maps.

2.3.3. Generating landcover change map

The eight forest-savanna maps were stacked to generate a transition map representing landcover change (or vegetation dynamics) between the years 1975 and 2020. Forests pre-existing in 1975 were grouped in a single class of forests older than 45 years (stable forests). Pixels that witnessed a permanent change from savanna (0) to forest (1) or the opposite were classified as "forest gain" or "forest loss" respectively and the year of detected transition was recorded. Pixels that underwent more than one transition throughout the monitoring period (i.e., 4% of the cases) were classified as "unstable dynamics" and discarded from the analysis.

2.3.4. Validation of landcover and landcover change maps and estimation of the area of land change

To assess the accuracy of landcover and landcover change maps and estimate the area of land change, we followed good practices guidelines detailed in Olofsson et al. (2014). In particular, the estimation of landcover maps accuracy was made using reference samples selected by stratified random sampling. For each binary forest-savanna map, 50 pixels were randomly drawn from each stratum and pixels' label (i.e. forest or savanna) was assigned by visual interpretation using the Landsat image of the year corresponding to the classification. The set of reference samples was then used to generate a confusion matrix and derive accuracy statistics (i.e. producer, user and overall accuracy), as described in section 4.3 of Olofsson et al. (2014).

The landcover change map was evaluated by assessing the accuracy of the dominant classes throughout the study period, namely stable forests (i.e., 2020's forests existing since 1975 or earlier), stable savannas, and forest gain (i.e., forests that appeared between 1975-2020). While forest loss (i.e., forests that transitioned to savannas between 1975-2020) was also observed in the landcover change map, it only concerned 0.2% of the pixels and was therefore discarded from the analysis. We randomly drew 100 pixels from each stable class and 200 pixels in the forest gain class, and followed the same procedure as for the binary maps to compute accuracy statistics.

To estimate the area of forest gain, we used two methodological approaches. The first approach consisted in simply counting pixels classified as "forest gain" in the landcover change map (i.e., so-called pixel-counting method, Waldner and Defourny, 2017) from which an area estimate could be derived. To warrant the unbiasedness of the estimate and assess the uncertainty around this estimate, we also followed the approach prescribed in Olofsson et al. (2014), namely using a probability sample and invoking design-based inference. In practice, the set of reference samples used to assess the accuracy of the landcover change map, together with the landcover change map itself, was used to estimate the area of forest gain from the samples.

2.4. Mapping fire frequency

The unsupervised 2-class clustering approach used to discriminate between forest and savanna could not be used to map fire scars, despite the conspicuous spectral signature of recent burns. Although the burn scars remain visible for weeks or more through time, their signature is progressively attenuating (Appendix B) and many images may not display scars. For the same reason, temporal image aggregates are useless, as fire scars are too transitory. We therefore needed to turn to a more traditional approach, based on a fixed spectral threshold applied to each image in the collection. Due to the sparsity of image series acquired before 1999 and the failure in the scan line corrector of Landsat 7 we limited the fire frequency analysis to Landsat 8 as from jan. 2014 to dec. 2018 before LC #8 (5 years; see Fig. 2B).

2.4.1. Mapping fires scars

Amongst the numerous vegetation indices used to characterize fire occurrence, the Normalized Burn Ratio (NBR, Key and Benson, 2003; Fig. 3) has gained consideration for detecting burn scars left after a fire (Escuin et al., 2008; Kane et al., 2014; Miller and Thode, 2007; Sunderman and Weisberg, 2011). The NBR index (equation 1) is calculated using reflectance data from

passive optical sensors, especially the near infrared (NIR) and Shortwave infrared (SWIR) bands:

$$NBR = \frac{(NIR-SWIR)}{(NIR+SWIR)} \quad \text{(eq. 1)}$$

NBR was computed for each pixel and each observation in their respective time series in GEE. We then adopted a semi-automated approach to map fire scars from the NBR time series. First, we haphazardly selected one Landsat 8 image with apparent fire scars and visually delineated polygons on burned and unburned areas in each image. Based on a visual assessment of NBR distributions in burned and unburned polygons, we fixed an NBR cut-off value of 0.1 to separate burned (NBR < 0.1) and unburned (NBR >= 0.1) pixels in the entire image collection (see Appendix B-a). This threshold of 0.1 was confirmed when observing the NBR variation with time (i.e. on other Landsat 8 images) for frequently and rarely burned pixels (Appendix B-b), which showed the progressive fading of fire scars' influence on pixel spectral properties. For each pixel, the result of this classification process was thus a time series - hereafter referred to as the fire scar time series - with observations classified as burned (presence of fire scar) or unburned (absence of fire scar) and featuring, for each observation, the associated image acquisition date.

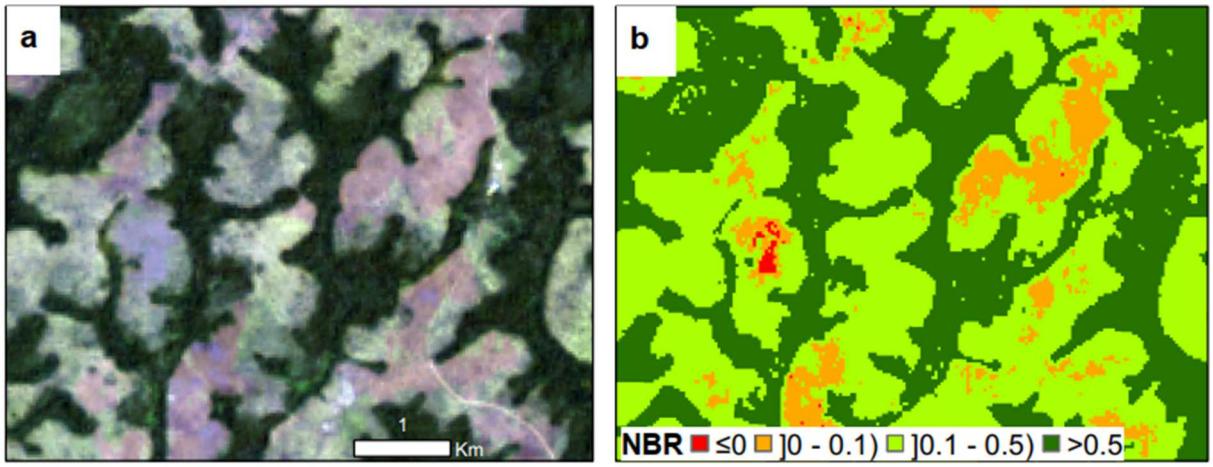

Fig. 3: Example of fire scar discrimination from the Normalized burn ratio (NBR). (**a**) RGB true colour composite of a forest-savanna landscape from Landsat 8 (LC08_186056_20191130). (**b**) NBR of the same area highlighting burn scars in red and orange with photosynthetically active savanna in light green and forest vegetation in darkgreen.

2.4.2. Quantifying fire frequency

We quantified the fire frequency by computing a Fire Frequency Index (FFI) from the fire scar time series. To account for the irregular distribution of spaceborne observations within and among years resulting from the filtering of cloudy or shadowed observations, we first

aggregated the information contained in pixels' fire scars time series into yearly observations. For a given pixel a year was considered as a "burned year" when the pixel was classified as fire scar for at least two consecutive observations. The FFI for a pixel was then computed as the ratio between the numbers of "burned years" over the total number of years in the fire monitoring period.

- Comparing Landsat- and MODIS-derived fire frequencies

The MODIS burned area monthly product (MCD64A1.006 Collection 6) at 500 m resolution (Boschetti et al., 2019) is a reference data source that we used for the sake of comparison with fire frequencies derived from Landsat. We computed FFI values of all burned pixels from MODIS burned area monthly product in the 2014-2018 fire monitoring period, and compared the distribution of areas (in km²) in each FFI class to the distribution derived from Landsat. The comparison aimed at assessing the interest of increased spatial resolution (i.e., 30 vs 500 m) for our understanding of forest-savanna dynamics.

2.5. Mapping current vegetation diversity and structure

2.5.1. Spectral composition gradients

The increase in spatial and spectral resolutions of open-access spaceborne images offers interesting prospects for the monitoring of biodiversity from space. The link between remotely sensed spectral information and ecological indicators of diversity was formulated by Palmer et al., (2002) and referred to as the spectral variation hypothesis (SVH). This hypothesis initially related the spatial variability in spectral information to environmental heterogeneity, and was used in various contexts in order to provide an estimation of species diversity (Rocchini et al., 2016, 2010). Féret and Asner (2014) developed a method aiming at computing diversity indicators directly from spectral information in order to compare them to the same diversity indicators derived from species field inventories, and used dissimilarity metrics as a proxy for tree taxonomic turnover. This methodology implemented in the biodivMapR R package (Féret and Boissieu, 2020) relies on the assumption that discrimination among species, or groups of species, can be obtained from the clustering of spectral information. The resulting clusters, named 'spectral species' by the authors, aim at defining optical types (Ustin and Gamon, 2010) with an unsupervised procedure. These optical types provide combined information on functional and taxonomic properties of vegetation. Here, we used this method to assess and map spectral composition gradients on a cloud free Sentinel 2 image of the dry season (27-01-2020; T32NQL & T32NRL). Although the analysis was performed on a local computer after

retrieving the Sentinel 2 image composite from Google Earth Engine, it is worth noting that biodivMapR can as well be implemented on the fly using an R interface on the Google cloud platform, thus alleviating the need for any local image data processing. We processed forest and savanna pixels separately, using the previously derived 2019-2020 landcover classification as a mask. Within a given landcover subset (i.e., forest or savanna) an unsupervised k-means clustering was used to assign individual pixels to spectral species based on their spectral signatures. Féret and Boissieu (2020) suggested using 40 - 50 spectral species to accommodate for the high diversity of tropical forests. However, using a large number of spectral species did not change the overall pattern of spectral composition gradients in our study area, and we thus set the number of spectral species to 10. The image was then gridded into 30 x 30 m windows (to match the spatial resolution of the Landsat-derived landcover change map) and the dissimilarity between each pair of windows was computed using the Bray-Curtis dissimilarity metric. Principal Coordinate Analysis (PCoA; Legendre and Legendre, 1998) was then applied on the resulting dissimilarity matrix and the first axis was retained to reflect turn-over in (spectral) species composition, for either savanna or forest ecosystems.

2.5.2. Aboveground biomass

LiDAR scanning technology has emerged as the reference approach for mapping variation of vegetation AGB at landscape scale (Colgan and Asner, 2014; Jha et al., 2020; Sagang et al., 2020) due to its ability to accurately characterize the vegetation's three-dimensional structure.

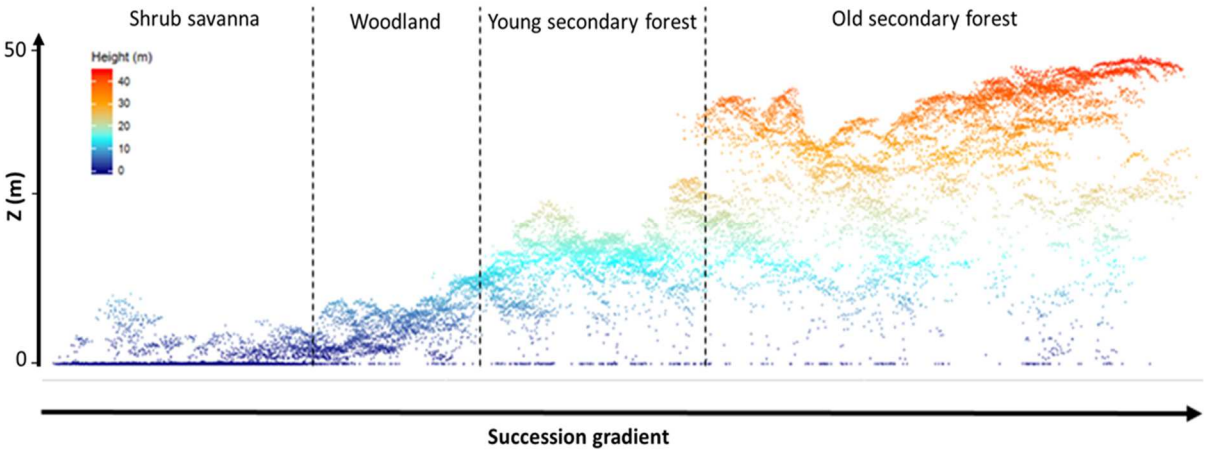

Fig. 4: Three-dimensional profile of the vegetation structure along a savanna to forest transitional gradient extracted from the UAV-borne LiDAR scanning data available in the study area. The profile corresponds to a 14 m thick extract.

We used a DJI Matrice 600 UAV to mount a Riegl mini VUX-1 UAV scanner encased in a YellowScan Vx-20 device and acquired 3D data of the vegetation in 2019. The scanner works at 100 kHz over 360 degrees, yielding a point location accuracy of 2.5 cm vertically, thanks to

differentially corrected DGNSS (post-processing with local base station) positions and readings from an Applanix 20 inertial station (IMU). Flight height was set to 70 m above ground (SRTM; DTM) level with an average ground speed of 8 $m.s^{-1}$. The scan angle was filtered down to ± 60°, yielding a band swath of 121 m and a 50% overlap between two adjacent flight lines, which resulted in an average point density of 10.5 $points.m^{-2}$. The UAV-borne sampling was collected over ≈ 300 ha and was designed to cover a transitional gradient from savannas to the oldest forest patches of the landscape (Fig. 4). Points were classified into ground and vegetation returns using progressive morphological filter (pmf) algorithm (Zhang et al., 2003) as implemented in the classify_ground() function of the lidR R package (Roussel et al., 2021). To filter non-ground returns, we ran the pmf algorithm using a sequence of window sizes (from 3 to 12 pixels every 3 pixels) and elevation difference thresholds (from 0.1 to 1.5 every 0.35, see Zhang et al., 2003 and Roussel et al., 2021 for details on the pmf algorithm and its implementation in lidR). We applied a continuous normalization of the non-ground point cloud through the interpolation of the elevation of every single point location using ground points with the normalize_height() function of the lidR R package. Interpolation was done using a k-nearest neighbor approach with an inverse-distance weighting (see Roussel et al., 2021). The normalized point cloud was used to generate a 1-m canopy height model (CHM), from which we predicted vegetation AGB at 40-m spatial resolution using a model calibrated in a forest-savanna mosaic of the same region (equation 2, from Sagang et al., 2020).

$$AGB = 6.27 + 8.52 \times CHM \quad \text{(eq. 2)}$$

with AGB in $Mg.ha^{-1}$ and CHM in m.

Further, we evaluated the rate of AGB uptake for young secondary forests (≤ 20 years; Ipcc, 2006) and all the transitory forests (< 45 years; forest that appeared between 1975 and 2020) by (i) resampling the AGB map from 40-m to the 30-m resolution at which vegetation dynamics was assessed, and (ii) adjusting a simple linear relationship between predicted AGB and forest age derived from the forest transition map. All the statistical analyses were done using the R statistical software (R Core Team, 2018).

3. Results

3.1. Tracking four decades of landcover change trajectory

Overall accuracies of automated forest-savanna classifications ranged from 85.78% (± 6.26) to 96.85% (± 3.57) with an average of 92.54% (± 4.72, Appendix C). The Landsat 2 acquisition of dec. 1975 (Fig. 5-a) shows that the MDNP was at that time dominated by savannas (c. 54%

of the park area; Fig. 6-a). After four decades of vegetation dynamics (see illustrative panels b and c in Fig. 5), the MDNP was, in 2020, dominated by forest (c. 72% of the park area; Fig. 6-a). Using binary forest-savanna classifications to assess landcover changes, the automated GEE routine suggested a 275 km² increase of forest area during the study period, which is consistent with the area estimate obtained from reference samples in a design-based inferential framework (i.e., 266 km² ± 26, Appendix D).

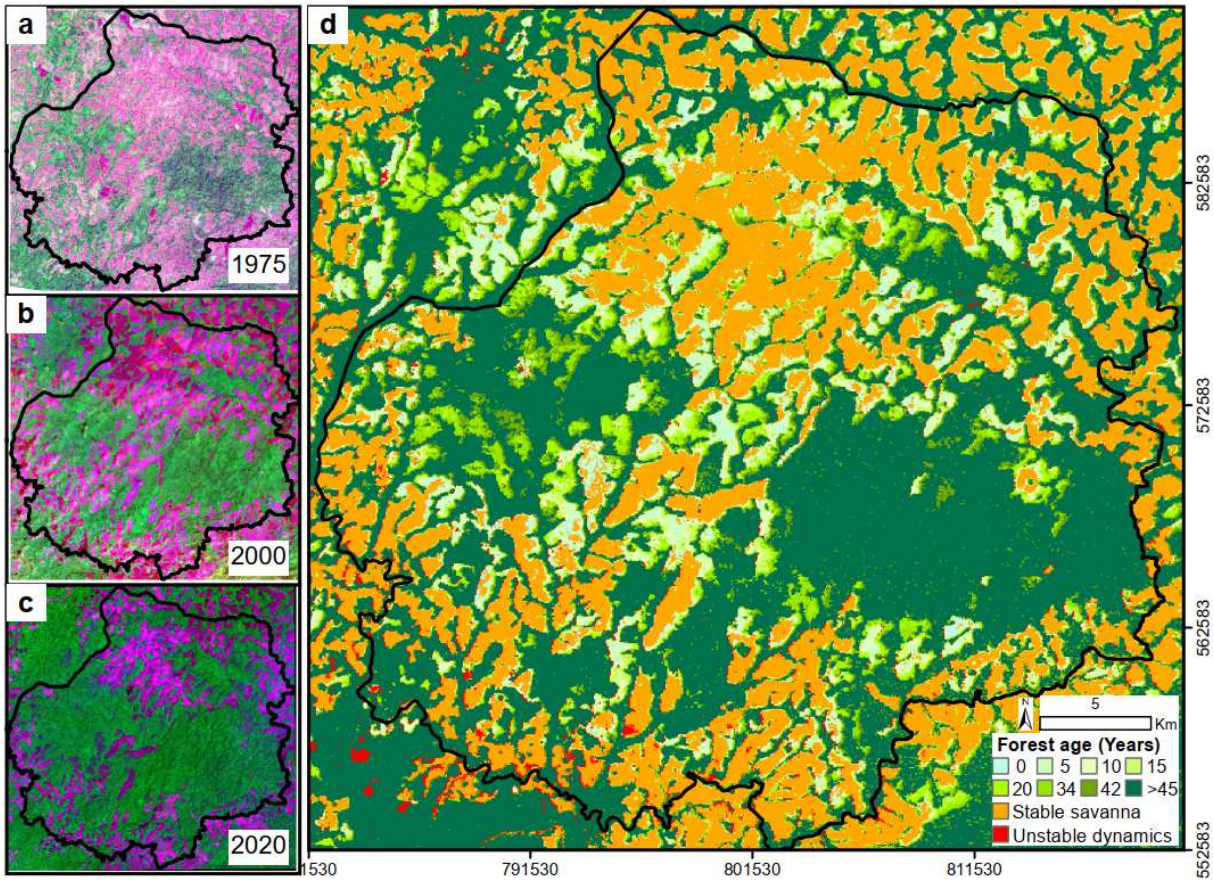

Fig. 5: Vegetation transition map of the Mpem & Djim National Park from 1975 to 2020. (**a**, **b**, **c**) illustrative Landsat images (RGB composition: Red-NIR-Green) for the years 1975, 2000 and 2020. Under this RGB composition, forests appear in green and savannas in purple. (**d**) Forest age map derived from the landcover classification at different dates.

The landcover change map depicted a consistent and regular pattern of forest progression into savanna (Fig. 6-a) and allowed deducing current forest age (displayed in Fig. 5-d) and average rate of forest progression. For instance, a weighted mean of forest encroachment rates obtained from successive classifications - using the length of monitoring periods as weights (vertical dashed bar in Fig. 6) - yield an average rate of 0.63%.year^{-1} or equivalently c. 6 km².year^{-1} (Fig. 6-b). Since 1975, the MDNP has thus lost about 50% of its initial savanna area, and linear extrapolation of forest cover change suggests that savannas will completely disappear from the park within the next 30 years.

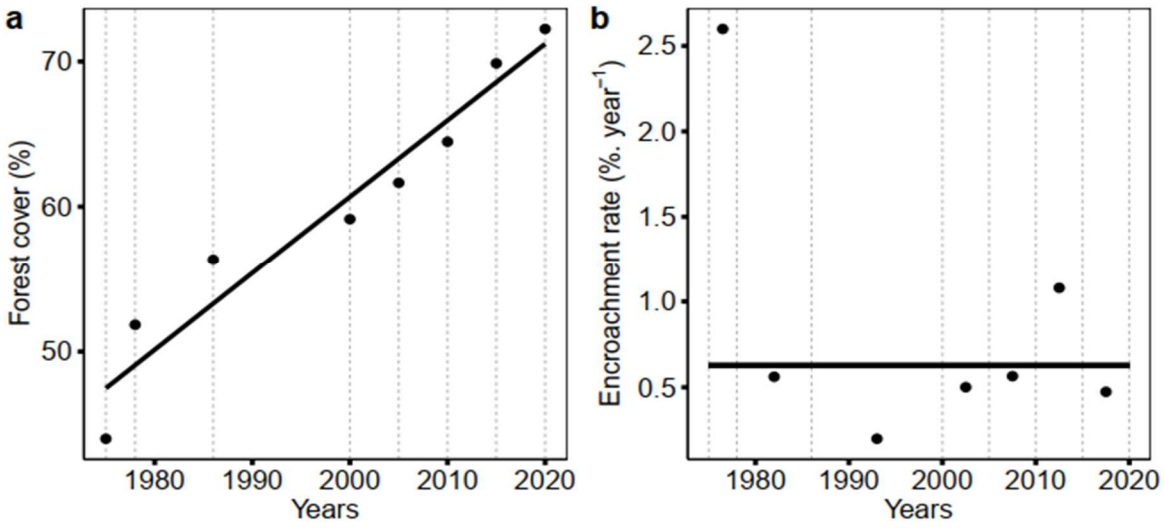

Fig. 6: Landcover change throughout the study period. (**a**) Variation of the proportion of forest cover over the years. Vertical gray dashed lines represent landcover classification dates and full black circles the forest cover estimate on each landcover map. The full black line represents the fit of a linear model. (**b**) Variation of forest encroachment rate between consecutive landcover classifications. The full black line represents a weighted mean of forest encroachment rates throughout the study period, using the time lengths between consecutive landcover classifications as weights.

3.2. Relationships between fire frequency and landcover change

Based on a visual interpretation we noticed that savannas surrounding the park principally in the northern part underwent higher fire frequencies as compared to the southern savannas (Fig. 7-a). Most of the savanna that transited to forest between two consecutive dates had an average Fire Frequency Index (FFI) of 0 in the 5 previous years (Fig. 7-b), meaning that no fire was detected. Persisting savanna that did not undergo any forest transition had a FFI presenting a broad range of FFI values.

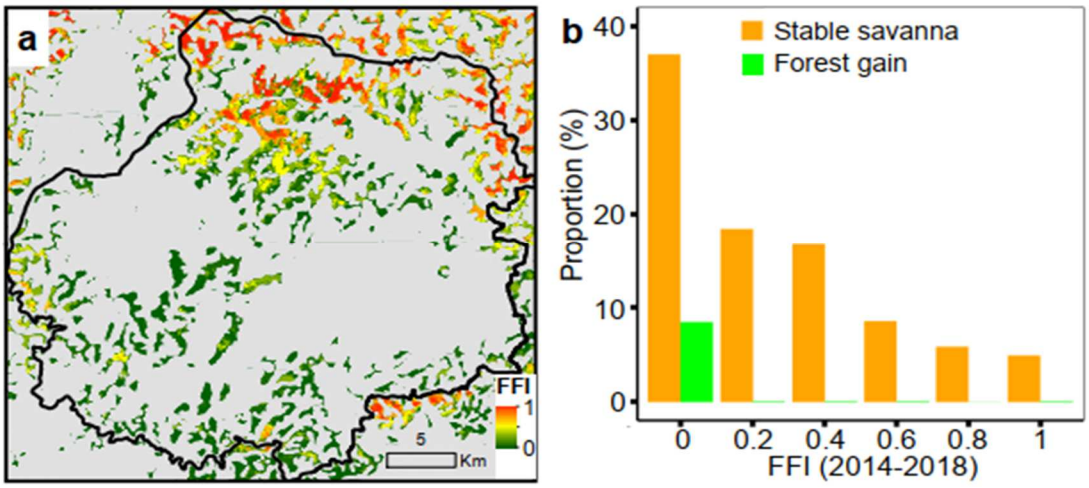

Fig. 7: Maps of the Fire Frequency Index (FFI) derived from Landsat 8 between 2014-2018 (**a**) with existing forests at the beginning of the monitoring period displayed in grey. (**b**) Associated barplots showing the distribution of FFI classes for stable savanna (orange) and forest gains (green) in consecutive landcover classifications.

3.3. Change in forest composition and structure with age

We assessed the relationships between forest age and (1) forest composition, indirectly characterized through spectral composition gradient analysis of 30 x 30 m windows spectral response and (2) forest structure, quantified by AGB estimates.

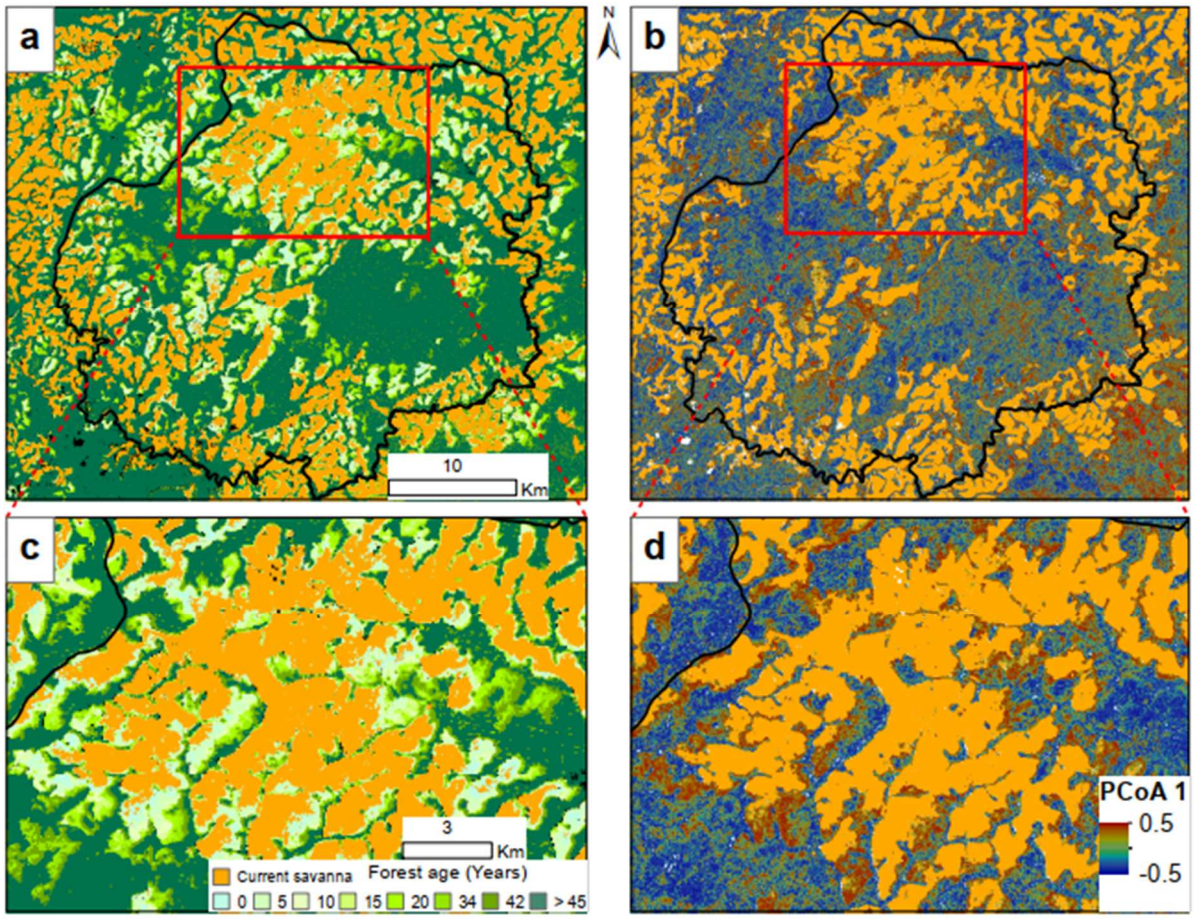

Fig. 8: Gradient of forest transition and the spatial distribution of the spectral composition over the study area. Forest age map (**a**) and (**b**) the spatial distribution of pixel scores along the first axis of a Principal Coordinate Analysis (PCoA 1 see section 2.5.1 for details). Negative PCoA values correspond to old growth forests while positive values correspond to young regrowth. (**c**) and (**d**) are subsets illustrating the area where the patterns are marked.

The first axis of the PCoA (PCoA 1) applied on the dissimilarity matrix computed from spectral species composition depicted a gradual change in forest composition from the forest-savanna edges (young forests in light green in Fig. 8-a & c with brown tone in Fig. 8-b & d) to the forest interior (old forests in dark green in Fig. 8-a & c with blue tone in Fig. 8-b & d). The spatial structure of forest spectral composition gradients matched the pattern of forest progression, with younger and older stands found on the positive and negative sides of PCoA 1 (Fig. 9-a), respectively.

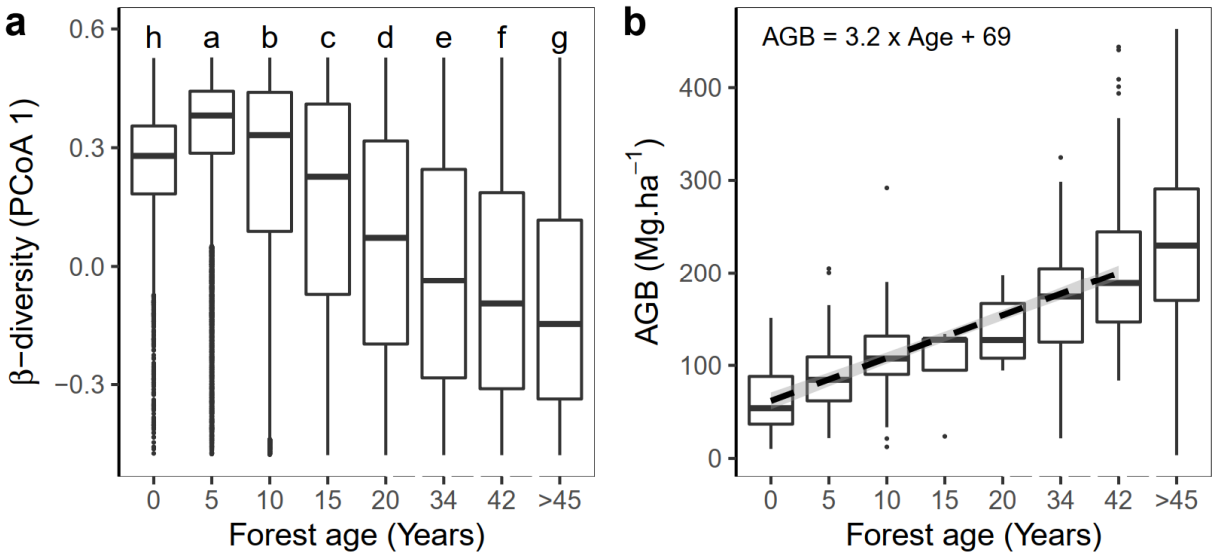

Fig. 9: Relationships between forest age, spectral composition and structure. (**a**) Boxplot of spectral composition derived from PCoA 1 (see section 2.5.1 for details), by forest age bins. Labelled letters represent the results of a Tukey honest significant difference (HSD) test, with different letters for boxes having different means at the probability cut-off value of $p < 0.05$. (**b**) Boxplot of pixels' aboveground biomass (AGB) by forest age bins. Dotted line represents the fit of a simple linear model between forest age and AGB for transitory forests (< 45 years) with its 95% confidence interval (grey ribbon). Note that in panels **a** and **b**, x axes after year 20 are represented with broken lines to mark a change in the interval between age bins.

It is worth noting that the variability (cf. e.g. the interquartile range in box plots) of spectral composition seemed to increase with age. We also observed consistent changes in forest structure (Fig. 9-b), with an increase in forest AGB from 61 ± 33 Mg.ha^{-1} for younger forests (less than 5 years since afforestation) up to 230 ± 80 Mg.ha^{-1} for the oldest forests (> 45 years). The transition map thus suggested an average linear increase of about 3.2 Mg.ha^{-1}.year^{-1} in MDNP forests since 1975 (Fig. 9-b). Young regenerating forests (≤ 20 years) seemed to show a higher AGB accumulation rate of 4.1 Mg.ha^{-1}.year^{-1} (not shown).

3.4. Change in savanna composition and structure with fire frequency

We investigated the relationships between the fire frequency of the past 5 years and the composition and structure of stable savannas (2020). Savanna spectral composition was consistent with the fire frequency (Fig. 10) and showed a marked bimodality along PCoA 1 with a clear segregation between the two extreme states (Fig. 11).

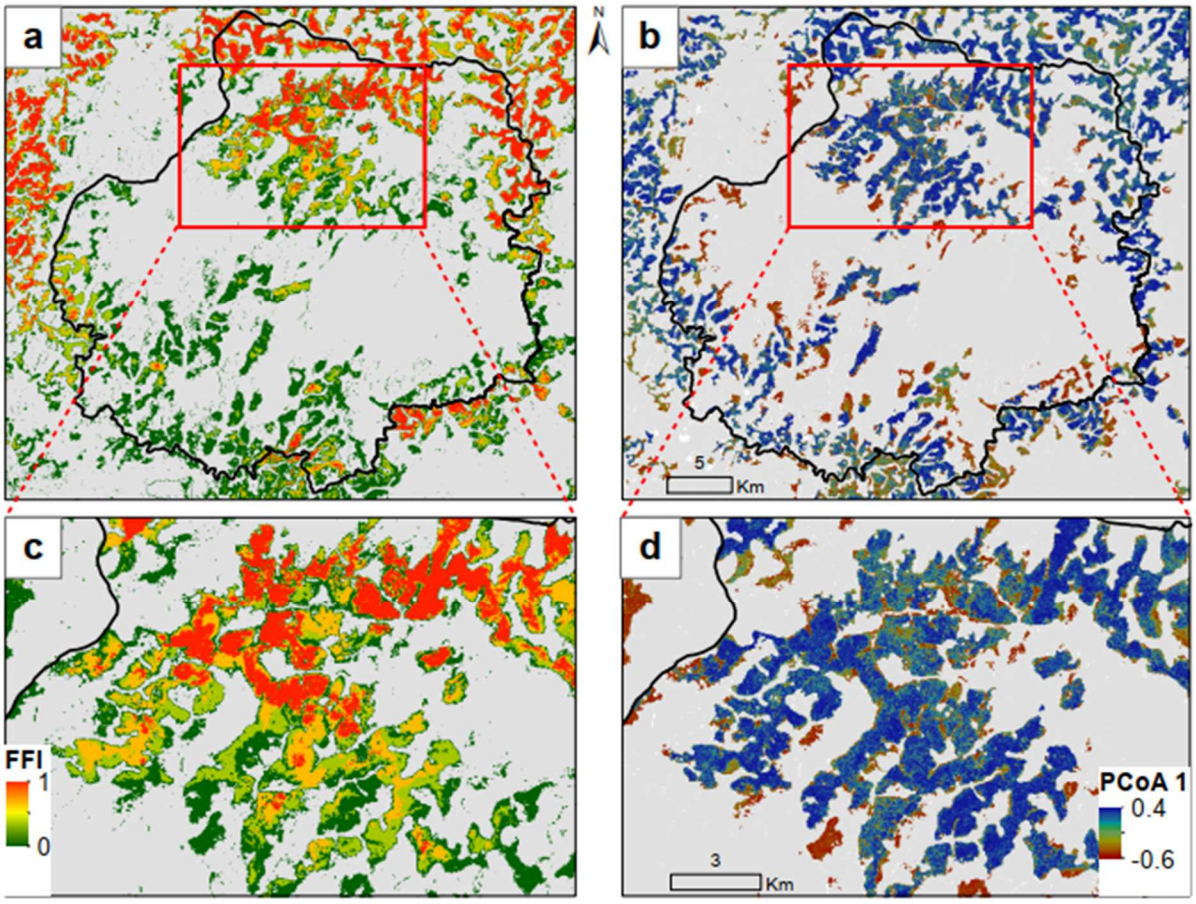

Fig. 10: Gradient of fire frequency and the spatial distribution of the spectral composition over persisting savannas the study area pixels from 1975 to 2020. Fire frequency map (**a**) and (**b**) the spatial distribution of pixel scores along the first axis of a Principal Coordinate Analysis (PCoA 1) over savannas. Negative PCoA values correspond to woody savanna while positive values correspond to grassy savanna. Forest pixels in 2020 are masked out (grey). (**c**) and (**d**) are subsets illustrating the area where the patterns are marked.

The spatial distribution of FFI was congruent with distribution patterns of spectral species composition opposing woody savanna (negative scores on PCoA 1 with a mode around ca.-0.6; Fig. 11-a) with higher AGB (c. 36 ± 27 $Mg.ha^{-1}$ for leftmost box in Fig. 11-b) and grassy savanna (positive scores on PCoA 1 with a mode around ca. 0.4; Fig. 11-a) with lower AGB (22 ± 18 $Mg.ha^{-1}$ for the rightmost box; Fig. 11-b). Woody savannas had rare fire events (FFI close to 0) while grassy savannas had higher fire frequencies (FFI close to 0.4).

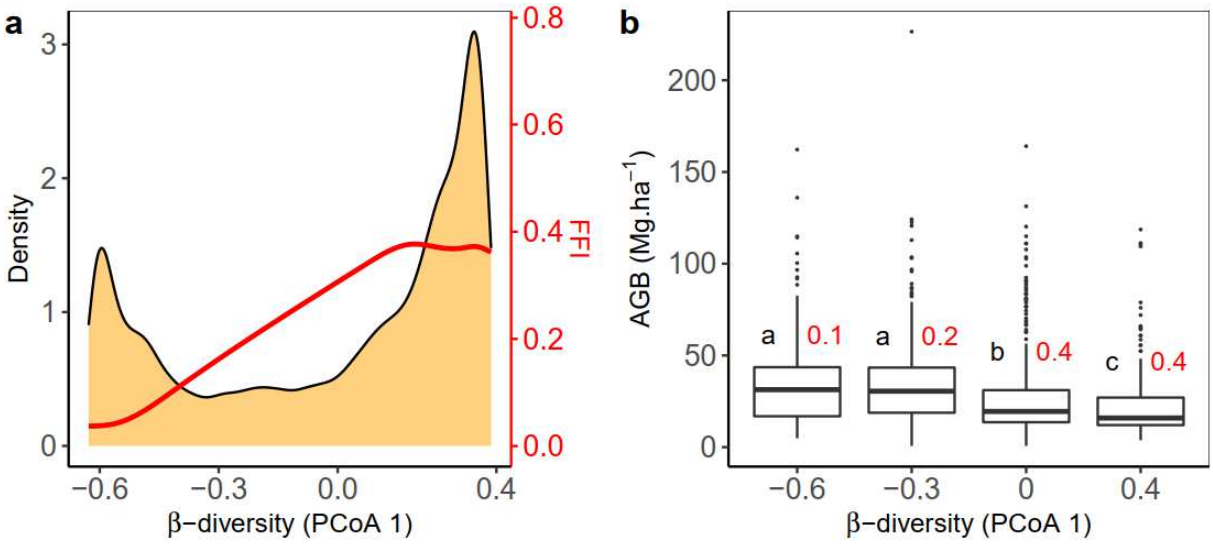

Fig. 11: Relationships between savanna spectral composition, fire frequency and savanna structure. (**a**) Density plot of spectral composition score on PCoA 1 and associated recent (2014-2018) fire frequency, represented by a smooth average of Fire Frequency Index (FFI; red line). (**b**) Boxplot of AGB variation by PCoA 1 bins. The labelled letters represent the results of a Tukey honest significant difference (HSD) test, with different letters for boxes having different means at the probability cut-off value of $p < 0.05$. Red numbers above the plots represent the average FFI for each PCoA 1 bin.

4. Discussion

4.1. Forest expansion

The FSE of northern hemisphere tropical Africa are currently experiencing woody encroachment and forest progression over savannas. Several studies, scattered from Guinea to the Central African Republic (Boulvert, 1990; Mitchard et al., 2011; Mitchard and Flintrop, 2013; Youta-Happi, 1998) and even central Gabon (Cardoso et al., 2020; Jeffery et al., 2014) have illustrated this trend, while referring to time windows of variable lengths within the last six decades (Aleman et al., 2017). However, in all documented sites, no methodologically consistent picture was available over more than 30 years. We show in the present study that simple principles for distinguishing contrasted vegetation types and fire occurrence regimes allow benefitting from massive high spatial resolution image series and cloud computing to consistently document the dynamics of forest-savanna boundaries. We indeed achieved an integrated picture of vegetation changes in a protected area in Central Cameroon (MDNP, ca. 1,000 km²) from 1975 to present, which is all over the timeframe covered by the Landsat series. Our characterization of forest progression qualitatively agrees with previous studies in nearby areas of the Guineo-Congolian region in Central Africa that stretched over either an early time window (50s – 90s, Youta-Happi, 2003) or a more recent one (1986 – 2006, Mitchard et al., 2009). Youta-Happi (2003) measured a forest encroachment rate of 0.74%.year^{-1} after 39 years

(1950-1989) of monitoring in a nearby area in Cameroon (Mbam et Kim confluent) using air photographs. Mitchard et al. (2009) expressed woody encroachment qualitatively as increases in canopy area index (CAI) computed using 3 images (1986, 2000, 2006), and observed a shrinking of low CAI areas (0.2 m²/m² area, interpreted as "grassy savanna") by 43% over 20 years (0.9% y^{-1} for 1986-2000 and 1.29% for 2000-2006). This trend was reported benefiting mostly to intermediate CAI classes (interpretable as both dense savanna and young forest) with a marginal increase of upper CAI class (>1 m²/m² which unequivocally relates to close canopy forest) (Mitchard et al., 2009). Hence their results suggest both forest expansion and woody biomass built-up in perpetuating savannas.

After forest transition, differences in the functional composition of plant communities are apparent in the spectral reflectance of forest canopies captured by Sentinel 2 satellite data. Spectral species composition appeared structured along a forest-age gradient. This reflects the successional gradient of floristic assemblages where fast growing pioneer species with low aboveground biomass yet strong photosynthetic activity dominate recent transitions and are then gradually replaced by long-lived species in old regenerating forests (Cuni-Sanchez et al., 2016; Deklerck et al., 2019; Ibanez et al., 2013; Youta-Happi et al., 2003). The fact that spectral variability increased with forest ages in our study area apparently contradicts findings by (Réjou-Méchain et al., 2014) in another context of Central African forests, where floristic variability assessed from field inventory data was found to be higher at the initial stages of succession. It may well be that the spectral signature, especially with a relatively low spectral resolution (compared to hyperspectral data at least) tends to group a number of similar species into broader functional groups (e.g. early pioneers; Laurin et al., 2016).

Thanks to the comparison between spaceborne image series and local UAV-borne LiDAR data we were able to quantify the pace of AGB increment from recent forest transitions to older forests. AGB was found to steadily increase with a hint of leveling-off after 20 years. Our rate of AGB increase of 4.1 $Mg.ha^{-1}.yr^{-1}$ found for young secondary forests (≤ 20 years as defined by IPCC) is 59% lower than the IPCC (2006) default AGB accumulation rate for young tropical rainforest in Africa (≈ 10 $Mg.ha^{-1}.year^{-1}$; Suarez et al., 2019). Refined IPCC 2006 default AGB accumulation rate proposed by Suarez et al. (2019) is still above our own estimate by 46% (7.6 ± 5.9 $Mg.ha^{-1}.yr^{-1}$). This would reflect a contrasted scenario of AGB uptake depending on whether the forest recovers after disturbances (reforestation) or encroaches over grassy and woody savanna (afforestation). The former regeneration process would imply an average AGB uptake 2-fold greater than in the latter scenario as compared to the Suarez et al. (2019)

estimates. The type of previous landcover or disturbance has been found elsewhere to significantly influence the carbon accumulation rate (Cook-Patton et al., 2020; Moran et al., 2000). Reforestation actually occurs on previously forested soils (Janzen, 2016), keeping characteristics (soil fertility and structural properties) favorable to forest seedlings establishment and growth (Viani et al., 2011). Afforestation on the other hand generally occurs on nutrient-poor savanna soils leading to a slower forest gain (Moran et al., 2000). This study focused on aboveground carbon stocks and no consideration was made to the carbon stored in soils which can be higher in grassy and woody savannas as compared to forests (Buisson et al., 2019; Silveira et al., 2020).

4.2. The role of fire in shaping savanna structure and dynamics

Mesic savannas represent alternative stable states to forest (Hirota et al., 2011; Staver et al., 2011a) in areas of intermediate rainfall (between 700 and 1900 mm/year for Africa; Aleman et al., 2020; Staver et al., 2011a), where savannas are maintained thanks to regular disturbances, notably by fire (Langevelde et al., 2003; Veenendaal et al., 2018; Venter et al., 2018). The MDNP being in the intermediate rainfall area, the observed forest progression might either be the result of a reduction of fire disturbances or to global climate change inducing locally wetter climatic conditions. As observed elsewhere, such as in La Lopé National Park (LLNP) in Gabon (Jeffery et al., 2014), fire frequency is not homogeneous across the landscape, because of variation in ignition sources or natural breaks. This heterogeneity translates in differential rates for woody encroachment and forest progression. In most cases, no fire occurrence was recorded during at least five years for pixels of woody savanna that transited to forest between the last two consecutive monitoring periods. Fire-free intervals facilitate tree recruitment and growth and allow trees to approach canopy closure which suppresses fire by excluding grasses (Bond and Midgley, 2000; Hirota et al., 2011; Staver et al., 2011b; Veenendaal et al., 2018, 2015). In LLNP savannas newly protected from fire can sufficiently thicken up over a 15 year period to reach a structure comparable to a colonizing forest (Jeffery et al., 2014). In the absence of fire, the system switches from a state of co-occurrence of fire-adapted trees and heliophytic grasses to a state with fire impervious, shade-bearing giant herbs (*Aframomum spp.)* and forbs (*Chromolaena odorata,* a well-known invasive woody weed; Youta-Happi, 1998; Oliveras and Malhi, 2016) along with saplings of light-demanding forest tree species such as *Albizia spp.*, *Macaranga spp.* (Ibanez et al., 2013; Youta-Happi, 1998; Youta-Happi et al., 2003; Youta-Happi and Bonvallot, 1996). Cardoso et al., (2020) evidenced the presence of an ecotone community in LLNP that occupies a narrow belt between savanna and forest and prevents fire

progression within the forest when savanna burn regularly. According to our floristic data from 61 0.16-ha field plots which analysis is beyond the scope of the present paper, the aforementioned community is also frequent in the ecotones of the MDNP and a similar role can be hypothesized.

The spectral diversity in the (currently remaining) savannas of our study site evidenced two contrasting dominant states either related to low (FFI ≈ 0) or high (FFI ≈ 0.4) fire frequencies. Interestingly, we observed a decreasing relationship between AGB and the fire frequency that led from high AGB (mean of ca. 36 $Mg.ha^{-1}$) with low fire frequencies (corresponding to woody savanna) to low AGB (ca. 22 $Mg.ha^{-1}$) with high fire frequency situations (corresponding to grassy savanna). This suggests that savannas with low fire frequency (FFI ≤ 0.2) accumulate ≈ 40% more AGB than those with high fire frequency. We may here note that we observed very few savannas displaying intermediate fire frequency (0.2-0.3.$year^{-1}$) and intermediate AGB (≈ 27 Mg/ha^{-1}). Analogously, Mitchard et al. (2009) found that savannas of intermediate CAI were relatively scarce in the nearby Mbam-Djerem region. Our results suggest that humid savannas seem to be the most unstable/prone to forest transition under a low fire frequency as the latter is not sufficient to prevent woody biomass build-up. Inversely, increased woody biomass and cover is known to depress grass production (Hoffmann et al., 2012; Veenendaal et al., 2018) that is the main fire fuel after drying-up, thereby indirectly limiting fire intensity and propagation (Lehmann et al., 2011). The shift towards woody savanna and associated ineffective fire regimes seems here to occur for AGB values around 27 $Mg.ha^{-1}$. Once this threshold is exceeded, the AGB build-up towards 36 $Mg.ha^{-1}$ (i.e. towards a woody savanna) seems inexorable and prefigures the progressive floristic shift towards stands dominated by forest pioneer species that displayed AGB values in the range 60 - 100 $Mg.ha^{-1}$. Field prospection allowed us to frequently observe dense woody savanna characterized by tall savanna trees (mainly *Terminalia glaucescens*) frequently fringing young forests dominated by species such as *Albizia adianthifolia* and *Macaranga spp.* that overtopped surviving *T. glaucescens* engulfed in dense thickets of *C. odorata*. All this strongly suggests recent afforestation. During the five years of fire monitoring (2014-2018) we noticed some persistent savannas (for which no forest transition was detected) with low fire frequency (FFI < 0.2). While not documented in this study, other factors may explain this savanna stability under low fire frequencies, such as topo-edaphic controls (Colgan et al., 2012), or fire characteristics (Jeffery et al., 2014; Walters, 2012).

4.3. Implications for conservation and management

The creation of the MDNP in 2004 may have hindered anthropogenic activities principally at its less accessible savanna core where we observed intense forest expansion. A lower proportion of forest transitions is observed in peripheral savannas, which are more accessible especially in the northern part of the MDNP where natural boundaries constituted by Mpem and Djim rivers are absent. From the various observations made during field campaigns conducted between 2019 and 2020; we noticed that those savannas were subject to substantial livestock transhumance during the dry season (Nov. - Mar.). During that period shepherds regularly burn the savanna to favor grass flush (Youta-Happi and Bonvallot, 1996; Mitchard et al., 2009). Poachers also set fire for the same reason, as well as to increase visibility or drive the game (as described by Walters, 2010). Frequent fires limit the growth of woody savanna species and woody build-up in savannas which makes the establishment of forest species unlikely (Dantas et al., 2013; Venter et al., 2018) and delays forest expansion. On the other hand, cattle grazing and trampling limit the accumulation of grass fuel and are liable to depress both fire frequency and intensity. Our results suggest that a quinquennial fire frequency (i.e., a fire event every five years) could constitute a tipping point between grassy savanna and woody savanna. Considering the dramatic forest expansion we evidenced, the current, unplanned fire regimes seem unable to preserve the mosaic landscape.

Our findings have important management implications as they provide insight into the ecological challenge associated with woody and forest encroachment, which is a pervasive phenomenon and a growing concern for managers of African savannas (Stevens et al., 2017; Venter et al., 2018). Fire frequency in the MDNP is generally the product of non-managed fires as the park still lacks an effective fire management program. Therefore, managers in the MDNP have little influence on how much of the park burns on an annual basis, and that area burned is largely dictated by uncontrolled actions from transhumant shepherds and poachers. Maintaining at least one or more fires every five years is necessary to ensure the maintenance of an open canopy cover. Forest expansion appeared indeed as a continuous and steady process in the MDNP and if we extrapolate the observed fairly constant rate of forest gain into savanna, the area may lose all its savanna in less than 30 years. This is even more certain when we consider the rise in CO_2 concentration and climate change predictions for tropical Africa that expect an increase in precipitation over the next decades (Pachauri and Meyer, 2014). Both events can influence the growth rate of juvenile plants, thereby affecting tree recruitment and the conversion of open savannas to woodlands (Bond and Midgley, 2012) favoring forest expansion (Bond and Midgley, 2012; Staver et al., 2011b; Stevens et al., 2017). Local factors including

fire management, soil fertility or hydromorphy and herbivory pressure are expected to mediate this general prediction. Although carbon mitigation programs such as REDD+ scheme tend to encourage forest expansion, the loss of savanna ecosystems in the area will drastically modify landscape-level diversity (Bond, 2016; Veldman, 2016) and ecosystem services, including hydrology (Acharya et al., 2018) and soil nutrient cycles (Berthrong et al., 2009), including soil carbon storage (Chiti et al., 2018; Cuni-Sanchez et al., 2016), and it would markedly alter community assemblages (Abreu et al., 2017; Bremer and Farley, 2010) especially those of savanna plant and animal specialists, including iconic large mammals and big cats. That is the reason why park authorities should aim at maintaining the mosaic of forest and humid savannas that pre-existed gazetting of the protected areas they are in charge of (Jeffery et al., 2014).

4.4. Progress in modelling landscape dynamics

We here demonstrated the potential of approaches based on open source imagery and cloud-based platforms such as Google Earth Engine for landcover change monitoring. This offer prospects for an improved measurement of national level aboveground carbon stocks (Sagang et al., 2020) and stock changes in forest-savanna transitional landscapes (in relation to Tier 2 and Tier 3 accuracy levels), in compliance with the United Nations Framework Convention on Climate Change (UNFCCC) and IPCC requirements for countries still reporting at Tier 1 level, as it is the case in Central Africa (Romijn et al., 2015). Localized airborne LiDAR data provide a good reference to map AGB variation over sufficiently large regions (Wulder et al., 2012) to allow upscaling using spaceborne data (Sagang et al., 2020). The FFI obtained in this study using 30 m Landsat was shown to better retrieve the variability of fire frequencies than the 500 m MODIS fire product. The latter indeed estimated FFI 28% lower than the former on average, and totally failed to detect areas with the highest frequency (yearly) of fire regime. This finding accords with Chuvieco et al. (2019) and Ramo et al. (2021) who found that recent BA products covering Africa with Sentinel-2 images (at 20 m spatial resolution) over a single year reached estimates 1.8 and 3.2 times higher, respectively, than the estimates from MODIS products. This strong discrepancy is mostly caused by insufficient spatial resolution leading to the omission of small fires (< 100 ha) (Roteta et al., 2019) as the study area is likely dominated by small low-intensity fires (Mitchard et al., 2009), in accordance with the fire biomes typology (Archibald et al., 2013). This raises a caveat considering that several studies (Axelsson and Hanan, 2018; Diouf et al., 2012; Staver et al., 2011b, 2011a; Venter et al., 2018) fully relied on MODIS to assess fire frequency influence on the vegetation structure. A limitation that needs to be pointed out in this study is that fire monitoring was restricted to yearly fire statistics, ignoring the

seasonality of fire within the year (early or late fires) despite known influence on savanna structure (Bucini and Lambin, 2002; Diouf et al., 2012). Subsequent efforts are therefore needed to temporally disaggregate annual FFI products. Another obvious perspective is to extend our approaches to other forest-savanna transition zones. Preliminary tests show that the open source algorithms proposed along with this publication should allow a smooth transposition, as long as the studied areas present vegetation mosaics having sufficiently distinct radiometric signatures.

5. Conclusion

We leveraged on the potential offered by open access satellite imagery and cloud computing facilities (GEE), as well as UAV-LiDAR data, to monitor complex forest-savanna biomass and compositional dynamics at a meaningful scale in the MDNP. Landsat image archives recorded a long-term (> 42 years) forest spread into savanna at a rate of ca. 0.63%.year^{-1}. The spectral assemblages of the forest cover characterized using Sentinel 2 multispectral imagery and AGB variations quantified using UAV-LiDAR data allowed map compositional and structural changes along the forest succession gradient and quantify rates of biomass accumulation. Fire occurrence, as recorded via the Landsat archive, modulated bush encroachment and forest expansion, with a five-year fire frequency found to be the threshold below which woody plants dominate and open the way to forest transition. These results highlight the importance of fire in maintaining savanna ecosystem in the area. These findings allow providing detailed information to support decision makers in charge of carbon sequestration and biodiversity conservation policies.

Acknowledgements

This work was financially supported by the Nachtigal Hydropower Company (Contract n◦ C006C007-DES-2017) under the environmental impact study associated to the construction of a hydroelectric dam on the Sanaga river in the Centre region of Cameroon. This study is also part of the 3DForMod project (ANR-17-EGAS-0002-01) funded by the framework of the JPI FACCE ERA-GAS call under the European Union's Horizon 2020 research and innovation program (grant agreement no. 696356). L.B.T.S. benefited from the "Allocations de recherche pour une thèse au Sud (ARTS)" grant program to fund research stays in France. J.B.F. acknowledges financial support from Agence Nationale de la Recherche (BioCop project-ANR-17-CE32-0001). We thank Clément Aubert for assistance in UAV-LiDAR data acquisition. We are grateful to Imma Tchefferi, Amélie Kunito and the MDNP staff officers for

699 assistance during field data collection. We thank the anonymous reviewers for their significant
700 comments and contributions to the manuscript.

701 Authors' contributions

702 L.B.T.S., and N.B. conceived and designed the experiments. L.B.T.S., P.P. and N.B. edited the
703 different GEE scripts. G.V. and J.B.F. helped with image processing using BiodivMapR.
704 L.B.T.S. performed the experiments and analysed the results, with the help of P.P., N.B. and
705 P.C. L.B.T.S. wrote the first drafts of the paper and N.B., P.C., P.P., G.V., B.S. and J.B.F.
706 contributed edits and advice on content. All authors have read and agreed to the published
707 version of the manuscript.

708 Data Accessibility

709 Data that support the findings of this study are available from the corresponding author upon
710 request. The forest transition and fire frequency raster and Google Earth Engine codes are
711 available here .

712 Orcid

713 Sagang Takougoum Le Bienfaiteur https://orcid.org/0000-0001-8778-3121
714 Ploton Pierre https://orcid.org/0000-0002-8800-3593
715 Viennois Gaëlle https://orcid.org/0000-0001-9772-343X
716 Jean-Baptiste Féret https://orcid.org/0000-0002-0151-1334
717 Sonké Bonaventure https://orcid.org/0000-0002-4310-3603
718 Couteron Pierre https://orcid.org/0000-0002-4627-1696
719 Nicolas Barbier https://orcid.org/0000-0002-5323-3866

720 References

721 Abreu, R.C.R., Hoffmann, W.A., Vasconcelos, H.L., Pilon, N.A., Rossatto, D.R., Durigan,
722 G., 2017. The biodiversity cost of carbon sequestration in tropical savanna. Sci. Adv. 3,
723 1–8.

724 Acharya, B.S., Kharel, G., Zou, C.B., Wilcox, B.P., Halihan, T., 2018. Woody plant
725 encroachment impacts on groundwater recharge: A review. Water.
726 https://doi.org/10.3390/w10101466

727 Aleman, J.C., Fayolle, A., Favier, C., Staver, A.C., Dexter, K.G., Ryan, C.M., Azihou, A.F.,
728 Bauman, D., Te Beest, M., Chidumayo, E.N., Comiskey, J.A., Cromsigt, J.P.G.M.,
729 Dessard, H., Doucet, J.-L., Finckh, M., Gillet, J.-F., Gourlet-Fleury, S., Hempson, G.P.,
730 Holdo, R.M., Kirunda, B., Kouame, F.N., Mahy, G., Gonçalves, F.M.P., McNicol, I.,
731 Quintano, P.N., Plumptre, A.J., Pritchard, R.C., Revermann, R., Schmitt, C.B.,
732 Swemmer, A.M., Talila, H., Woollen, E., Swaine, M.D., 2020. Floristic evidence for
733 alternative biome states in tropical Africa. Proc. Natl. Acad. Sci. U. S. A. 1–8.
734 https://doi.org/10.1073/pnas.2011515117

735 Aleman, J.C., Jarzyna, M.A., Staver, A.C., 2017. Forest extent and deforestation in tropical
736 Africa since 1900. Nat. Ecol. Evol. 2, 26–33. https://doi.org/10.1038/s41559-017-0406-1

737 Archibald, S., Lehmann, C.E.R., Gomez-Dans, J.L., Bradstock, R. a, 2013. Defining pyromes
738 and global syndromes of fire regimes. Proc. Natl. Acad. Sci. 110, 6442–6447.
739 https://doi.org/10.1073/pnas.1211466110

740 Axelsson, C.R., Hanan, N.P., 2018. Rates of woody encroachment in African savannas reflect
741 water constraints and fire disturbance. J. Biogeogr. 45, 1209–1218.
742 https://doi.org/10.1111/jbi.13221

743 Banskota, A., Kayastha, N., Falkowski, M.J., Wulder, M.A., Froese, R.E., White, J.C., 2014.
744 Forest Monitoring Using Landsat Time Series Data: A Review. Can. J. Remote Sens. 40,
745 362–384. https://doi.org/10.1080/07038992.2014.987376

746 Bastin, J.F., Finegold, Y., Garcia, C., Mollicone, D., Rezende, M., Routh, D., Zohner, C.M.,
747 Crowther, T.W., 2019. The global tree restoration potential. Science (80-.). 364, 76–79.
748 https://doi.org/10.1126/science.aax0848

749 Beer, C., Reichstein, M., Tomelleri, E., Ciais, P., Jung, M., Carvalhais, N., Rödenbeck, C.,
750 Arain, M.A., Baldocchi, D., Bonan, G.B., Bondeau, A., Cescatti, A., Lasslop, G.,

751 Lindroth, A., Lomas, M., Luyssaert, S., Margolis, H., Oleson, K.W., Roupsard, O.,
752 Veenendaal, E., Viovy, N., Williams, C., Woodward, F.I., Papale, D., 2010. Terrestrial
753 gross carbon dioxide uptake: Global distribution and covariation with climate. Science
754 (80-.). 329, 834–838. https://doi.org/10.1126/science.1184984

755 Berthrong, S.T., Jobbágy, E.G., Jackson, R.B., 2009. A global meta-analysis of soil
756 exchangeable cations, pH, carbon, and nitrogen with afforestation. Ecol. Appl. 19, 2228–
757 2241. https://doi.org/10.1890/08-1730.1

758 Blaum, N., Rossmanith, E., Popp, A., Jeltsch, F., 2007. Shrub encroachment affects
759 mammalian carnivore abundance and species richness in semiarid rangelands. Acta
760 Oecologica 31, 86–92. https://doi.org/10.1016/J.ACTAO.2006.10.004

761 Bond, W.J., 2016. Ancient grasslands at risk. Science (80-.). 351, 120–122.
762 https://doi.org/10.1126/science.aad5132

763 Bond, W.J., Midgley, G.F., 2012. Carbon dioxide and the uneasy interactions of trees and
764 savannah grasses. Philos. Trans. R. Soc. B Biol. Sci. 367, 601–612.
765 https://doi.org/10.1098/rstb.2011.0182

766 Bond, W.J., Midgley, G.F., 2000. A proposed CO2-controlled mechanism of woody plant
767 invasion in grasslands and savannas. Glob. Chang. Biol. 6, 865–869.

768 Boschetti, L., Roy, D.P., Giglio, L., Huang, H., Zubkova, M., Humber, M.L., 2019. Global
769 validation of the collection 6 MODIS burned area product. Remote Sens. Environ. 235,
770 111490. https://doi.org/10.1016/j.rse.2019.111490

771 Boulvert, Y., 1990. Avancée ou recul de la forêt centrafricaine : changements climatiques,
772 influence de l'homme et notamment des feux, in: Paysages Quaternaires de l'Afrique
773 Centrale Atlantique. Paris, pp. 353–366.

774 Bremer, L.L., Farley, K.A., 2010. Does plantation forestry restore biodiversity or create green
775 deserts? A synthesis of the effects of land-use transitions on plant species richness.
776 Biodivers. Conserv. 19, 3893–3915. https://doi.org/10.1007/s10531-010-9936-4

777 Buisson, E., Le Stradic, S., Silveira, F.A.O., Durigan, G., Overbeck, G.E., Fidelis, A.,
778 Fernandes, G.W., Bond, W.J., Hermann, J.M., Mahy, G., Alvarado, S.T., Zaloumis, N.P.,
779 Veldman, J.W., 2019. Resilience and restoration of tropical and subtropical grasslands,
780 savannas, and grassy woodlands. Biol. Rev. 94, 590–609.

781 https://doi.org/10.1111/brv.12470

782 Cardoso, A.W., Oliveras, I., Abernethy, K.A., Jeffery, K.J., Glover, S., Lehmann, D., Edzang
783 Ndong, J., White, L.J.T., Bond, W.J., Malhi, Y., 2020. A distinct ecotonal tree
784 community exists at central African forest–savanna transitions. J. Ecol. 00, 1–14.
785 https://doi.org/10.1111/1365-2745.13549

786 Cava, M.G.B., Pilon, N.A.L., Priante, C.F., Ribeiro, M.C., Durigan, G., 2020. The recovery
787 rates of secondary savannas in abandoned pastures are poorly explained by
788 environmental and landscape factors. Appl. Veg. Sci. 23, 14–25.
789 https://doi.org/10.1111/avsc.12457

790 Cava, M.G.B., Pilon, N.A.L., Ribeiro, M.C., Durigan, G., 2018. Abandoned pastures cannot
791 spontaneously recover the attributes of old-growth savannas. J. Appl. Ecol. 55, 1164–
792 1172.

793 Chiti, T., Rey, A., Jeffery, K., Lauteri, M., Mihindou, V., Malhi, Y., Marzaioli, F., White,
794 L.J.T., Valentini, R., 2018. Contribution and stability of forest-derived soil organic
795 carbon during woody encroachment in a tropical savanna. A case study in Gabon. Biol.
796 Fertil. Soils 54, 897–907. https://doi.org/10.1007/s00374-018-1313-6

797 Chuvieco, E., Mouillot, F., van der Werf, G.R., San Miguel, J., Tanasse, M., Koutsias, N.,
798 García, M., Yebra, M., Padilla, M., Gitas, I., Heil, A., Hawbaker, T.J., Giglio, L., 2019.
799 Historical background and current developments for mapping burned area from satellite
800 Earth observation. Remote Sens. Environ. 225, 45–64.
801 https://doi.org/10.1016/j.rse.2019.02.013

802 Colgan, M.S., Asner, G.P., 2014. Coexistence and environmental filtering of species-specific
803 biomass in an African savanna. Ecology 95, 1579–1590. https://doi.org/10.1890/13-
804 1160.1

805 Colgan, M.S., Asner, G.P., Levick, S.R., Martin, R.E., 2012. Topo-edaphic controls over
806 woody plant biomass in South African savannas. Biogeosciences 9, 1809–1821.
807 https://doi.org/10.5194/bg-9-1809-2012

808 Cook-Patton, S.C., Leavitt, S.M., Gibbs, D., Harris, N.L., Lister, K., Anderson-Teixeira, K.J.,
809 Briggs, R.D., Chazdon, R.L., Crowther, T.W., Ellis, P.W., Griscom, H.P., Herrmann, V.,
810 Holl, K.D., Houghton, R.A., Larrosa, C., Lomax, G., Lucas, R., Madsen, P., Malhi, Y.,
811 Paquette, A., Parker, J.D., Paul, K., Routh, D., Roxburgh, S., Saatchi, S., van den

812 Hoogen, J., Walker, W.S., Wheeler, C.E., Wood, S.A., Xu, L., Griscom, B.W., 2020.
813 Mapping carbon accumulation potential from global natural forest regrowth. Nature 585,
814 545–550. https://doi.org/10.1038/s41586-020-2686-x

815 Cuni-Sanchez, A., White, L.J.T., Calders, K., Jeffery, K.J., Abernethy, K., Burt, A., Disney,
816 M., Gilpin, M., Gomez-Dans, J.L., Lewis, S.L., 2016. African savanna-forest boundary
817 dynamics: A 20-year study. PLoS One 11, 1–23.
818 https://doi.org/10.1371/journal.pone.0156934

819 Daldegan, G.A., de Carvalho Júnior, O.A., Guimarães, R.F., Gomes, R.A.T., Ribeiro, F. de F.,
820 McManus, C., 2014. Spatial patterns of fire recurrence using remote sensing and GIS in
821 the Brazilian savanna: Serra do Tombador Nature Reserve, Brazil. Remote Sens. 6,
822 9873–9894. https://doi.org/10.3390/rs6109873

823 Daldegan, G.A., Roberts, D.A., Ribeiro, F. de F., 2019. Spectral mixture analysis in Google
824 Earth Engine to model and delineate fire scars over a large extent and a long time-series
825 in a rainforest-savanna transition zone. Remote Sens. Environ. 232, 15pp.
826 https://doi.org/10.1016/j.rse.2019.111340

827 Dantas, V. de L., Batalha, M.A., Pausas, J., 2013. Fire drives functional thresholds on the
828 savanna – forest transition. Ecology 94, 2454–2463.

829 Deklerck, V., De Mil, T., Ilondea, B.A., Nsenga, L., De Caluwé, C., Van den Bulcke, J., Van
830 Acker, J., Beeckman, H., Hubau, W., 2019. Rate of forest recovery after fire exclusion
831 on anthropogenic savannas in the Democratic Republic of Congo. Biol. Conserv. 233,
832 118–130. https://doi.org/10.1016/j.biocon.2019.02.027

833 DeVries, B., Verbesselt, J., Kooistra, L., Herold, M., 2015. Robust monitoring of small-scale
834 forest disturbances in a tropical montane forest using Landsat time series. Remote Sens.
835 Environ. 161, 107–121. https://doi.org/10.1016/j.rse.2015.02.012

836 Dinerstein, E., Joshi, A.R., Vynne, C., Lee, A.T.L., Pharand-Deschênes, F., França, M.,
837 Fernando, S., Birch, T., Burkart, K., Asner, G.P., Olson, D., 2020. A “global safety net”
838 to reverse biodiversity loss and stabilize earth’s climate. Sci. Adv. 6, 13pp.
839 https://doi.org/10.1126/sciadv.abb2824

840 Diouf, A., Barbier, N., Lykke, A.M., Couteron, P., Deblauwe, V., Mahamane, A., Saadou, M.,
841 Bogaert, J., 2012. Relationships between fire history , edaphic factors and woody
842 vegetation structure and composition in a semi-arid savanna landscape (Niger , West

Africa). Appl. Veg. Sci. 15, 488–500. https://doi.org/10.1111/j.1654-109X.2012.01187.x

Djoufack, M.V., 2011. Étude multi-échelles des précipitations et du couvert végétal au Cameroun : Analyses spatiales, tendances temporelles, facteurs climatiques et anthropiques de variabilité du NDVI. PhD Thesis. Université de Bourgogne et Université de Yaoundé I. 321pp. Thesis. Université de Bourgogne et Université de Yaoundé I.

Duncanson, E.L., Disney, M., Armston, J., Nickeson, J., Minor, D., 2021. Committee on Earth Observation Satellites Working Group on Calibration and Validation Land Product Validation Subgroup Aboveground Woody Biomass Product Validation Good Practices Protocol 0–236. https://doi.org/10.5067/doc/ceoswgcv/lpv/agb.001

Dutrieux, L.P., Verbesselt, J., Kooistra, L., Herold, M., 2015. Monitoring forest cover loss using multiple data streams, a case study of a tropical dry forest in Bolivia. ISPRS J. Photogramm. Remote Sens. 107, 112–125. https://doi.org/10.1016/j.isprsjprs.2015.03.015

Escuin, S., Navarro, R., Fernández, P., 2008. Fire severity assessment by using NBR (Normalized Burn Ratio) and NDVI (Normalized Difference Vegetation Index) derived from LANDSAT TM/ETM images. Int. J. Remote Sens. 29, 1053–1073. https://doi.org/10.1080/01431160701281072

Estes, L., Elsen, P.R., Treuer, T., Ahmed, L., 2018. The spatial and temporal domains of modern ecology. Nat. Ecol. Evol. · 2, 819–826. https://doi.org/10.1038/s41559-018-0524-4

Féret, J.-B., Asner, G.P., 2014. Mapping tropical forest canopy diversity using high-fidelity imaging spectroscopy. Ecol. Appl. 24, 1289–1296.

Féret, J., Boissieu, F. de, 2020. biodivMapR: An r package for α- and β-diversity mapping using remotely sensed images. Methods Ecol. Evol. 11, 64–70. https://doi.org/10.1111/2041-210X.13310

Gómez, C., White, J.C., Wulder, M.A., 2016. Optical remotely sensed time series data for land cover classification : A review. ISPRS J. Photogramm. Remote Sens. 116, 55–72. https://doi.org/10.1016/j.isprsjprs.2016.03.008

Gorelick, N., Hancher, M., Dixon, M., Ilyushchenko, S., Thau, D., Moore, R., 2017. Google

873 Earth Engine: Planetary-scale geospatial analysis for everyone. Remote Sens. Environ.
874 202, 18–27. https://doi.org/10.1016/j.rse.2017.06.031

875 Grabska, E., Hostert, P., Pflugmacher, D., Ostapowicz, K., 2019. Forest stand species
876 mapping using the sentinel-2 time series. Remote Sens. 11, 1–24.
877 https://doi.org/10.3390/rs11101197

878 Hansen, M.C., Potapov, P. V, Moore, R., Hancher, M., Turubanova, S.A., Tyukavina, A.,
879 2013. High-Resolution Global Maps of 21st-Century Forest Cover Change. Science (80-.
880). 342, 850–854.

881 Hermosilla, T., Wulder, M.A., White, J.C., Coops, N.C., Hobart, G.W., 2015. An integrated
882 Landsat time series protocol for change detection and generation of annual gap-free
883 surface re fl ectance composites. Remote Sens. Environ. 158, 220–234.
884 https://doi.org/10.1016/j.rse.2014.11.005

885 Hirota, M., Holmgren, M., Nes, E.H. Van, Scheffer, M., 2011. Global Resilience of Tropical
886 Forest and Savanna to Critical Transitions. Science (80-.). 334, 232–235.
887 https://doi.org/10.1126/SCIENCE.1210657

888 Hoffmann, W.A., Geiger, E.L., Gotsch, S.G., Rossatto, D.R., Silva, L.C.R., Lau, O.L.,
889 Haridasan, M., Franco, A.C., 2012. Ecological thresholds at the savanna-forest
890 boundary: How plant traits, resources and fire govern the distribution of tropical biomes.
891 Ecol. Lett. 15, 759–768. https://doi.org/10.1111/j.1461-0248.2012.01789.x

892 Ibanez, T., Munzinger, J., Gaucherel, C., Curt, T., Hély, C., 2013. Inferring savannah-
893 rainforest boundary dynamics from vegetation structure and composition: A case study
894 in New Caledonia. Aust. J. Bot. 61, 128–138. https://doi.org/10.1071/BT12255

895 Ipcc, 2006. 2006 IPCC Guidelines for National Greenhouse Gas Inventories, Prepared by the
896 National Greenhouse Gas Inventories Programme, Eggleston H.S., Buendia L., Miwa K.,
897 Ngara T. and Tanabe K. (eds). Hayama, Japan.

898 Janzen, H.H., 2016. The Soil Remembers. Soil Sci. Soc. Am. J. 80, 1429–1432.
899 https://doi.org/10.2136/sssaj2016.05.0143

900 Jeffery, K.J., Korte, L., Palla, F., Walters, G., White, L.J.T., Abernethy, K.A., 2014. Fire
901 management in a changing landscape: A case study from Lopé national park, Gabon.
902 Parks 20, 39–52. https://doi.org/10.2305/IUCN.CH.2014.PARKS-20-1.KJJ.en

Jha, N., Tripathi, N.K., Chanthorn, W., Brockelman, W., Nathalang, A., Pélissier, R., Pimmasarn, S., Ploton, P., Sasaki, N., Virdis, S.G.P., Réjou-Méchain, M., 2020. Forest aboveground biomass stock and resilience in a tropical landscape of Thailand. Biogeosciences 17, 121–134. https://doi.org/https://doi.org/10.5194/bg-17-121-2020

Kane, V.R., North, M.P., Lutz, J.A., Churchill, D.J., Roberts, S.L., Smith, D.F., McGaughey, R.J., Kane, J.T., Brooks, M.L., 2014. Assessing fire effects on forest spatial structure using a fusion of Landsat and airborne LiDAR data in Yosemite National Park. Remote Sens. Environ. 151, 89–101. https://doi.org/https://doi.org/10.1016/j.rse.2013.07.041

Key, C.H., Benson, N.C., 2003. The Normalized Burn Ratio (NBR): A Landsat TM radiometric measure of burn severity. US Geol. Surv. North. Rocky Mt. Sci. Center. U.S. Dep. Inter. U.S. Geol. Surv. North. Rocky Mt. Sci. Center.

Langevelde, V.F., Van De Vijver, C.A.D.M., Kumar, L., Van De Koppel, J., De Ridder, N., Van Andel, J., Skidmore, A.K., Hearne, J.W., Stroosnijder, L., Bond, W.J., Prins, H.H.T., Rietkerk, M., 2003. Effects of fire and herbivory on the stability of savanna ecosystems. Ecology 84, 337–350.

Laurin, V.G., Puletti, N., Hawthorne, W., Liesenberg, V., Corona, P., Papale, D., Chen, Q., Valentini, R., 2016. Discrimination of tropical forest types, dominant species, and mapping of functional guilds by hyperspectral and simulated multispectral Sentinel-2 data. Remote Sens. Environ. 176, 163–176. https://doi.org/10.1016/j.rse.2016.01.017

Legendre, P., Legendre, L.F.J., 1998. Numerical ecology. Elsevier.

Lehmann, C.E.R., Archibald, S.A., Hoffmann, W.A., Bond, W.J., 2011. Deciphering the distribution of the savanna biome. New Phytol. 191, 197–209. https://doi.org/10.1111/j.1469-8137.2011.03689.x

Letouzey, R., 1985. Carte phytogéographique du Cameroun, 1:500 000, 8 feuillets + 5 notices. Institut de la Carte Internationale de la Végétation, Toulouse, France.

Liu, J., Heiskanen, J., Maeda, E.E., Pellikka, P.K.E., 2018. Burned area detection based on Landsat time series in savannas of southern Burkina Faso. Int. J. Appl. Earth Obs. Geoinf. 64, 210–220. https://doi.org/https://doi.org/10.1016/j.jag.2017.09.011

Ma, X., Mahecha, M.D., Migliavacca, M., van der Plas, F., Benavides, R., Ratcliffe, S., Kattge, J., Richter, R., Musavi, T., Baeten, L., Barnoaiea, I., Bohn, F.J., Bouriaud, O.,

933 Bussotti, F., Coppi, A., Domisch, T., Huth, A., Jaroszewicz, B., Joswig, J., Pabon-
934 Moreno, D.E., Papale, D., Selvi, F., Laurin, G.V., Valladares, F., Reichstein, M., Wirth,
935 C., 2019. Inferring plant functional diversity from space: the potential of Sentinel-2.
936 Remote Sens. Environ. 233, 111368. https://doi.org/10.1016/j.rse.2019.111368

937 Machida, W.S., Gomes, L., Moser, P., Castro, I.B., Miranda, S.C., da Silva-Júnior, M.C.,
938 Bustamante, M.M.C., 2021. Long term post-fire recovery of woody plants in savannas of
939 central Brazil. For. Ecol. Manage. 493, 119255.
940 https://doi.org/10.1016/j.foreco.2021.119255

941 Miller, J.D., Thode, A.E., 2007. Quantifying burn severity in a heterogeneous landscape with
942 a relative version of the delta Normalized Burn Ratio (dNBR). Remote Sens. Environ.
943 109, 66–80. https://doi.org/https://doi.org/10.1016/j.rse.2006.12.006

944 Mitchard, E.T.A., Flintrop, C.M., 2013. Woody encroachment and forest degradation in sub-
945 Saharan Africa ' s woodlands and savannas 1982 – 2006. Philos. Trans. R. Soc. B Biol.
946 Sci. 368, 1–7. https://doi.org/http://dx.doi.org/10.1098/rstb.2012.0406

947 Mitchard, E.T.A., Saatchi, S.S., Gerard, F.F., Lewis, S.L., Meir, P., 2009. Measuring woody
948 encroachment along a forest-savanna boundary in Central Africa. Earth Interact. 13,
949 29pp. https://doi.org/10.1175/2009EI278.1

950 Mitchard, E.T.A., Saatchi, S.S., Lewis, S.L., Feldpausch, T.R., Woodhouse, I.H., Sonké, B.,
951 Rowland, C., Meir, P., 2011. Measuring biomass changes due to woody encroachment
952 and deforestation / degradation in a forest – savanna boundary region of central Africa
953 using multi-temporal L-band radar backscatter. Remote Sens. Environ. 115, 2861–2873.
954 https://doi.org/10.1016/j.rse.2010.02.022

955 Moran, E.F., Brondizio, E.S., Tucker, J.M., da Silva-Forsberg, M.C., McCracken, S., Falesi,
956 I., 2000. Effects of soil fertility and land-use on forest succession in Amazônia. For.
957 Ecol. Manage. 139, 93–108. https://doi.org/10.1016/S0378-1127(99)00337-0

958 Nguyen, T.H., Jones, S., Soto-Berelov, M., Haywood, A., Hislop, S., 2020. Landsat time-
959 series for estimating forest aboveground biomass and its dynamics across space and
960 time: A review. Remote Sens. 12, 1–25. https://doi.org/10.3390/RS12010098

961 Niklas, K.J., Spatz, H.C., 2010. Worldwide correlations of mechanical properties and green
962 wood density. Am. J. Bot. 97, 1587–1594. https://doi.org/10.3732/ajb.1000150

963 Oliveras, I., Malhi, Y., 2016. Many shades of green: the dynamic tropical forest–savannah
964 transition zones. Philos. Trans. R. Soc. Biol. Sci. 371, 15pp.
965 https://doi.org/10.1098/rstb.2015.0308

966 Olofsson, P., Foody, G.M., Herold, M., Stehman, S. V., Woodcock, C.E., Wulder, M.A.,
967 2014. Good practices for estimating area and assessing accuracy of land change. Remote
968 Sens. Environ. 148, 42–57. https://doi.org/10.1016/j.rse.2014.02.015

969 Pachauri, R.., Meyer, L.A., 2014. Climate Change 2014: Synthesis Report. Contribution of
970 Working Groups I, II and III to the Fifth Assessment Report of the Intergovernmental
971 Panel on Climate Change. Geneva, Switzerland.

972 Palmer, M.W., Earls, P.G., Hoagland, B.W., White, P.S., Wohlgemuth, T., 2002. Quantitative
973 tools for perfecting species lists, in: Environmetrics. John Wiley & Sons, Ltd, pp. 121–
974 137. https://doi.org/10.1002/env.516

975 Panshin, A.J., De Zeeuw, C., 1980. Textbook of wood technology : structure, identification,
976 properties, and uses of the commercial woods of the United States and Canada. McGraw-
977 Hill.

978 R Core Team, 2018. R: A language and environment for statistical computing. R Foundation
979 for Statistical Computing.

980 Ramo, R., Roteta, E., Bistinas, I., van Wees, D., Bastarrika, A., Chuvieco, E., van der Werf,
981 G.R., 2021. African burned area and fire carbon emissions are strongly impacted by
982 small fires undetected by coarse resolution satellite data. Proc. Natl. Acad. Sci. 118,
983 e2011160118. https://doi.org/10.1073/pnas.2011160118

984 Réjou-Méchain, M., Flores, O., Pélissier, R., Fayolle, A., Fauvet, N., Gourlet-Fleury, S.,
985 2014. Tropical tree assembly depends on the interactions between successional and soil
986 filtering processes. Glob. Ecol. Biogeogr. 23, 1440–1449.
987 https://doi.org/10.1111/geb.12222

988 Rocchini, D., Balkenhol, N., Carter, G.A., Foody, G.M., Gillespie, T.W., He, K.S., Kark, S.,
989 Levin, N., Lucas, K., Luoto, M., Nagendra, H., Oldeland, J., Ricotta, C., Southworth, J.,
990 Neteler, M., 2010. Remotely sensed spectral heterogeneity as a proxy of species
991 diversity: Recent advances and open challenges. Ecol. Inform. 5, 318–329.
992 https://doi.org/10.1016/j.ecoinf.2010.06.001

Rocchini, D., Boyd, D.S., Féret, J.B., Foody, G.M., He, K.S., Lausch, A., Nagendra, H., Wegmann, M., Pettorelli, N., 2016. Satellite remote sensing to monitor species diversity: potential and pitfalls. Remote Sens. Ecol. Conserv. 2, 25–36. https://doi.org/10.1002/rse2.9

Romijn, E., Lantican, C.B., Herold, M., Lindquist, E., Ochieng, R., Wijaya, A., Murdiyarso, D., Verchot, L., 2015. Assessing change in national forest monitoring capacities of 99 tropical countries. For. Ecol. Manage. 352, 109–123. https://doi.org/10.1016/j.foreco.2015.06.003

Roteta, E., Bastarrika, A., Padilla, M., Storm, T., Chuvieco, E., 2019. Development of a Sentinel-2 burned area algorithm: Generation of a small fire database for sub-Saharan Africa. Remote Sens. Environ. 222, 1–17. https://doi.org/10.1016/j.rse.2018.12.011

Roussel, J.-R., David, A., Florian, D.B., Anderw, S.M., Jean-François, B., Demetrios, G., Steinmeier, L., Stanislaw Adaszewski, 2021. Package ‘ lidR .’

Rüger, N., Condit, R., Dent, D.H., DeWalt, S.J., Hubbell, S.P., Lichstein, J.W., Lopez, O.R., Wirth, C., Farrior, C.E., 2020. Demographic trade-offs predict tropical forest dynamics. Science (80-.). 368, 165–168. https://doi.org/10.1126/science.aaz4797

Sagang, L.B.T., Ploton, P., Sonké, B., Poilvé, H., Couteron, P., Barbier, N., 2020. Airborne Lidar Sampling Pivotal for Accurate Regional AGB Predictions from Multispectral Images in Forest-Savanna Landscapes. Remote Sens. 12, 20pp. https://doi.org/doi:10.3390/rs12101637

Sankaran, M., Hanan, N.P., Scholes, R.J., Ratnam, J., Augustine, D.J., Cade, B.S., Gignoux, J., Higgins, S.I., Le Roux, X., Ludwig, F., Ardo, J., Banyikwa, F., Bronn, A., Bucini, G., Caylor, K.K., Coughenour, M.B., Diouf, A., Ekaya, W., Feral, C.J., February, E.C., Frost, P.G.H., Hiernaux, P., Hrabar, H., Metzger, K.L., Prins, H.H.T., Ringrose, S., Sea, W., Tews, J., Worden, J., Zambatis, N., 2005. Determinants of woody cover in African savannas. Nature 438, 846–849. https://doi.org/10.1038/nature04070

Santoir, C., Bopda, A., 1995. Atlas régional Sud-Cameroun.

Santoro, M., Cartus, O., Carvalhais, N., Rozendaal, D., Avitabile, V., Araza, A., De Bruin, S., Herold, M., Quegan, S., Rodr\’\iguez-Veiga, P., others, 2021. The global forest above-ground biomass pool for 2010 estimated from high-resolution satellite observations. Earth Syst. Sci. Data 13, 3927–3950.

1024 Silveira, F.A.O., Arruda, A.J., Bond, W., Durigan, G., Fidelis, A., Kirkman, K., Oliveira,
1025 R.S., Overbeck, G.E., Sansevero, J.B.B., Siebert, F., Siebert, S.J., Young, T.P., Buisson,
1026 E., 2020. Myth-busting tropical grassy biome restoration. Restor. Ecol. 28, 1067–1073.
1027 https://doi.org/10.1111/REC.13202

1028 Sirami, C., Seymour, C., Midgley, G., Barnard, P., 2009. The impact of shrub encroachment
1029 on savanna bird diversity from local to regional scale. Divers. Distrib. 15, 948–957.
1030 https://doi.org/10.1111/J.1472-4642.2009.00612.X

1031 Sosef, M.S.M., Dauby, G., Blach-Overgaard, A., van der Burgt, X., Catarino, L., Damen, T.,
1032 Deblauwe, V., Dessein, S., Dransfield, J., Droissart, V., Duarte, M.C., Engledow, H.,
1033 Fadeur, G., Figueira, R., Gereau, R.E., Hardy, O.J., Harris, D.J., de Heij, J., Janssens, S.,
1034 Klomberg, Y., Ley, A.C., Mackinder, B.A., Meerts, P., van de Poel, J.L., Sonké, B.,
1035 Stévart, T., Stoffelen, P., Svenning, J.C., Sepulchre, P., Zaiss, R., Wieringa, J.J.,
1036 Couvreur, T.L.P., 2017. Exploring the floristic diversity of tropical Africa. BMC Biol.
1037 15, 1–23. https://doi.org/10.1186/s12915-017-0356-8

1038 Souverijns, N., Buchhorn, M., Horion, S., Fensholt, R., Verbeeck, H., Verbesselt, J., Herold,
1039 M., Tsendbazar, N.-E., Bernardino, P.N., Somers, B., Van De Kerchove, R., 2020. Thirty
1040 Years of Land Cover and Fraction Cover Changes over the Sudano-Sahel Using Landsat
1041 Time Series. Remote Sens. 12. https://doi.org/10.3390/rs12223817

1042 Staver, A.C., Archibald, S., Levin, S., 2011a. Tree cover in sub-Saharan Africa : Rainfall and
1043 fire constrain forest and savanna as alternative stable states. Ecol. Stud. 92, 1063–1072.

1044 Staver, A.C., Archibald, S., Levin, S.A., 2011b. The Global Extent and Determinants of
1045 Savanna and Forest as Alternative Biome States. Science (80-.). 334, 230–232.
1046 https://doi.org/10.1126/science.1210465

1047 Stevens, N., Erasmus, B.F.N., Archibald, S., Bond, W.J., 2016. Woody encroachment over 70
1048 years in South African savannahs: Overgrazing, global change or extinction aftershock?
1049 Philos. Trans. R. Soc. Biol. Sci. 371, 9pp. https://doi.org/10.1098/rstb.2015.0437

1050 Stevens, N., Lehmann, C.E.R., Murphy, B.P., Durigan, G., 2017. Savanna woody
1051 encroachment is widespread across three continents. Glob. Chang. Biol. 23, 235–244.
1052 https://doi.org/10.1111/gcb.13409

1053 Suarez, D.R., Phillips, O.L., Rozendaal, D.M.A., Sy, V. De, Dávila, E.A., Teixeira, K.A.,
1054 Araujo, A., Luzmila, M., Timothy, A., Frans, R.B., Griscom, B.W., Carter, S., Cook,

S.C., Ted, P., Harris, N., Hérault, B., Leavitt, S.M., Lewis, S.L., N, J.K., Guessan, A.E.N., Sist, P., Mendoza, A.M., Sonké, B., Sullivan, M.J.P., Wang, M.M.H., Martius, C., Vilanova, E., Herold, M., 2019. Estimating aboveground net biomass change for tropical and subtropical forests : Refinement of IPCC default rates using forest plot data. Glob. Chang. Biol. 3609–3624. https://doi.org/10.1111/gcb.14767

Sullivan, M.J.P., TalbDiversity and carbon storage across the tropical forest biomeot, J., Lewis, S.L., Phillips, O.L., Qie, L., Begne, S.K., Chave, J., Cuni-Sanchez, A., Hubau, W., Lopez-Gonzalez, G., Miles, L., Monteagudo-Mendoza, A., Sonké, B., Sunderland, T., Ter Steege, H., White, L.J.T., Affum-Baffoe, K., Aiba, S.I., De Almeida, E.C., De Oliveira, E.A., Alvarez-Loayza, P., Dávila, E.Á., Andrade, A., Aragão, L.E.O.C., Ashton, P., Aymard, G.A., Baker, T.R., Balinga, M., Banin, L.F., Baraloto, C., Bastin, J.F., Berry, N., Bogaert, J., Bonal, D., Bongers, F., Brienen, R., Camargo, J.L.C., Cerón, C., Moscoso, V.C., Chezeaux, E., Clark, C.J., Pacheco, Á.C., Comiskey, J.A., Valverde, F.C., Coronado, E.N.H., Dargie, G., Davies, S.J., De Canniere, C., Djuikouo, M.N., Doucet, J.L., Erwin, T.L., Espejo, J.S., Ewango, C.E.N., Fauset, S., Feldpausch, T.R., Herrera, R., Gilpin, M., Gloor, E., Hall, J.S., Harris, D.J., Hart, T.B., Kartawinata, K., Kho, L.K., Kitayama, K., Laurance, S.G.W., Laurance, W.F., Leal, M.E., Lovejoy, T., Lovett, J.C., Lukasu, F.M., Makana, J.R., Malhi, Y., Maracahipes, L., Marimon, B.S., Junior, B.H.M., Marshall, A.R., Morandi, P.S., Mukendi, J.T., Mukinzi, J., Nilus, R., Vargas, P.N., Camacho, N.C.P., Pardo, G., Peña-Claros, M., Pétronelli, P., Pickavance, G.C., Poulsen, A.D., Poulsen, J.R., Primack, R.B., Priyadi, H., Quesada, C.A., Reitsma, J., Réjou-Méchain, M., Restrepo, Z., Rutishauser, E., Salim, K.A., Salomão, R.P., Samsoedin, I., Sheil, D., Sierra, R., Silveira, M., Slik, J.W.F., Steel, L., Taedoumg, H., Tan, S., Terborgh, J.W., Thomas, S.C., Toledo, M., Umunay, P.M., Gamarra, L.V., Vieira, I.C.G., Vos, V.A., Wang, O., Willcock, S., Zemagho, L., 2017. Diversity and carbon storage across the tropical forest biome. Sci. Rep. 7. https://doi.org/10.1038/srep39102

Sunderman, S.O., Weisberg, P.J., 2011. Remote sensing approaches for reconstructing fire perimeters and burn severity mosaics in desert spring ecosystems. Remote Sens. Environ. 115, 2384–2389. https://doi.org/10.1016/j.rse.2011.05.001

Thomas, C.D., Anderson, B.J., Moilanen, A., Eigenbrod, F., Heinemeyer, A., Quaife, T., Roy, D.B., Gillings, S., Armsworth, P.R., Gaston, K.J., 2013. Reconciling biodiversity and carbon conservation. Ecol. Lett. 16, 39–47. https://doi.org/10.1111/ele.12054

USGS, 2020. United States Geological Survey. Science for a changing world [WWW Document]. URL https://earthexplorer.usgs.gov/

Ustin, S.L., Gamon, J.A., 2010. Remote sensing of plant functional types. New Phytol. https://doi.org/10.1111/j.1469-8137.2010.03284.x

Valentini, R., Arneth, A., Bombelli, A., Castaldi, S., Cazzolla Gatti, R., Chevallier, F., Ciais, P., Grieco, E., Hartmann, J., Henry, M., Houghton, R.A., Jung, M., Kutsch, W.L., Malhi, Y., Mayorga, E., Merbold, L., Murray-Tortarolo, G., Papale, D., Peylin, P., Poulter, B., Raymond, P.A., Santini, M., Sitch, S., Vaglio Laurin, G., van der Werf, G.R., Williams, C.A., Scholes, R.J., 2014. A full greenhouse gases budget of Africa: synthesis, uncertainties, and vulnerabilities. Biogeosciences 11, 381–407. https://doi.org/10.5194/bg-11-381-2014

Veenendaal, E.M., Feldpausch, T.R., Domingues, T.F., Gerard, F., Schrodt, F., Saiz, G., Quesada, C.A., Djagbletey, G., Ford, A., Kemp, J., Marimon, B.S., Lenza, E., Ratter, J.A., Maracahipes, L., Sasaki, D., Zapfack, L., Villarroel, D., Schwarz, M., Ishida, F.Y., Gilpin, M., Nardoto, G.B., Arroyo, L., Bloomfield, K., Ceca, G., Compaore, H., Davies, K., Diallo, A., Fyllas, N.M., Gignoux, J., Hien, F., Johnson, M., Mougin, E., Hiernaux, P., Killeen, T., Metcalfe, D., Miranda, H.S., Steininger, M., Sykora, K., Bird, M.I., Grace, J., Lewis, S., Phillips, O.L., Lloyd, J., 2015. Structural , physiognomic and above-ground biomass variation in savanna – forest transition zones on three continents – how different are co-occurring savanna and forest formations ? Biogeosciences 12, 2927–2951. https://doi.org/10.5194/bg-12-2927-2015

Veenendaal, E.M., Torello-Raventos, M., Miranda, H.S., Sato, N.M., Oliveras, I., Langevelde, F., Asner, G.P., Lloyd, J., 2018. On the relationship between fire regime and vegetation structure in the tropics. New Phytol. 218, 153–166. https://doi.org/10.1111/NPH.14940

Veldman, J.W., 2016. Clarifying the confusion : old-growth savannahs and tropical ecosystem degradation. Philos. Trans. R. Soc. B Biol. Sci. 371, 11.

Veldman, J.W., Overbeck, G.E., Negreiros, D., Mahy, G., Le Stradic, S., Fernandes, G.W., Durigan, G., Buisson, E., Putz, F.E., Bond, W.J., 2015. Where Tree Planting and Forest Expansion are Bad for Biodiversity and Ecosystem Services. Bioscience 65, 1011–1018. https://doi.org/10.1093/biosci/biv118

Venter, Z.S., Cramer, M.D., Hawkins, H.J., 2018. Drivers of woody plant encroachment over

Africa. Nat. Commun. 9, 1–7. https://doi.org/10.1038/s41467-018-04616-8

Verbesselt, J., Hyndman, R., Newnham, G., Culvenor, D., 2010. Detecting trend and seasonal changes in satellite image time series. Remote Sens. Environ. 114, 106–115. https://doi.org/10.1016/j.rse.2009.08.014

Viani, R.A.G., Rodrigues, R.R., Dawson, T.E., Oliveira, R.S., 2011. Savanna soil fertility limits growth but not survival of tropical forest tree seedlings. Plant Soil 349, 341–353. https://doi.org/10.1007/s11104-011-0879-7

Waldner, F., Defourny, P., 2017. Where can pixel counting area estimates meet user-defined accuracy requirements? Int. J. Appl. Earth Obs. Geoinf. 60, 1–10. https://doi.org/https://doi.org/10.1016/j.jag.2017.03.014

Walters, G., 2012. Customary Fire Regimes and Vegetation Structure in Gabon's Bateke Plateaux. Hum. Ecol. 40, 943–955. https://doi.org/10.1007/s10745-012-9536-x

Wulder, M.A., White, J.C., Nelson, R.F., Næsset, E., Ørka, H.O., Coops, N.C., Hilker, T., Bater, C.W., Gobakken, T., 2012. Lidar sampling for large-area forest characterization: A review. Remote Sens. Environ. 121, 196–209. https://doi.org/10.1016/j.rse.2012.02.001

Xie, Z., Phinn, S.R., Game, E.T., Pannell, D.J., Hobbs, R.J., Briggs, P.R., McDonald-Madden, E., 2019. Using Landsat observations (1988–2017) and Google Earth Engine to detect vegetation cover changes in rangelands - A first step towards identifying degraded lands for conservation. Remote Sens. Environ. 232, 111317. https://doi.org/10.1016/j.rse.2019.111317

Youta-Happi, J., 1998. Arbres contre graminées : la lente invasion de la savane par la forêt au Centre-Cameroun. PhD Thesis. Université De Paris-Sorbone (PARIS IV). 241 p. Thesis. Université De Paris-Sorbone (PARIS IV).

Youta-Happi, J., Bonvallot, J., 1996. La disparition des savanes au Centre Cameroun entre 1950 et 1990, in: CNRS-ORSTOM (Ed.), Dynamique à Long Terme Des Écosystèmes Forestiers Intertropicaux. Paris, France, p. 3.

Youta-Happi, J., Bonvallot, J., Hotyat, M., Guillet, B., Peltre, P., Schwartz, D., Servant, M., Simonneaux, V., 2003. Bilan de la dynamique du contact forêt-savane en quarante ans (1950-1990) Dans la région du confluent du Mbam et du Kim, Centre-Cameroun, in:

IRD, É. (Ed.), Peuplements Anciens et Actuels Des Forêts Tropicales. p. 380 p. https://doi.org/10.4000/books.irdeditions.1486

Zeng, Z., Piao, S., Chen, A., Lin, X., Nan, H., Li, J., Ciais, P., 2013. Committed changes in tropical tree cover under the projected 21st century climate change. Sci. Rep. 3, 1951. https://doi.org/10.1038/srep01951

Zhang, K., Chen, S., Whitman, D., Shyu, M., Yan, J., 2003. A Progressive Morphological Filter for Removing Nonground Measurements From Airborne LIDAR Data 41, 872–882.